

Review

Open Access



# Recent advances in high temperature solid oxide electrolytic cells

Wei Chen, Chunwen Sun\*

School of Chemical and Environmental Engineering, China University of Mining & Technology (Beijing), Beijing 100083, China.

\*Correspondence to: Dr. Chunwen Sun, School of Chemical and Environmental Engineering, China University of Mining & Technology (Beijing), No. Ding 11, Xueyuan Road, Haidian District, Beijing 100083, China. E-mail: csun@cumtb.edu.cn

**How to cite this article:** Chen, W.; Sun, C. Recent advances in high temperature solid oxide electrolytic cells. *Energy Mater.* 2025, 5, 500045. <https://dx.doi.org/10.20517/energymater.2024.144>

**Received:** 30 Aug 2024 **First Decision:** 31 Oct 2024 **Revised:** 20 Nov 2024 **Accepted:** 5 Dec 2024 **Published:** 19 Feb 2025

**Academic Editor:** Sining Yun **Copy Editor:** Fangling Lan **Production Editor:** Fangling Lan

## Abstract

Solid oxide electrolytic cells (SOECs) with oxygen ion- or proton-conducting electrolytes have received extensive attention in recent years as a kind of energy storage technology. SOECs achieve the synthesis of chemicals such as hydrogen, CO or syngas by electrolyzing water, CO<sub>2</sub> or both at high temperatures. This review presents the basic structure and electrochemical principle of SOECs, then introduces the recent research progress of cathodes, anodes and electrolytes in SOECs, and particularly points out the current challenges of SOEC materials, such as inactivation at high temperatures and decay due to long-term operation. We summarize various strategies to improve the properties of different electrode materials, including doping, *in situ* exsolution and microstructure modification. Moreover, the advantages and disadvantages of different SOEC stack structures (planar and tubular) are also outlined. Finally, the future development trends in novel materials and engineering design of SOECs are proposed.

**Keywords:** Solid oxide electrolytic cells, perovskite cathodes, hydrogen production, degradation mechanisms, SOEC stacks

## INTRODUCTION

At present, the global energy structure is still dominated by traditional fossil energy sources, which cause serious environmental pollution. With the increasing demand for clean energy, hydrogen (H<sub>2</sub>) as an efficient and environmentally friendly energy carrier has received widespread attention<sup>[1]</sup>. Traditional



© The Author(s) 2025. **Open Access** This article is licensed under a Creative Commons Attribution 4.0 International License (<https://creativecommons.org/licenses/by/4.0/>), which permits unrestricted use, sharing, adaptation, distribution and reproduction in any medium or format, for any purpose, even commercially, as long as you give appropriate credit to the original author(s) and the source, provide a link to the Creative Commons license, and indicate if changes were made.



hydrogen production technology is mainly based on the reforming and partial oxidation of fossil fuels, which not only consumes a large amount of energy but also produces a lot of carbon dioxide. Therefore, the development of clean and efficient hydrogen production technology has become a hot research topic today. As shown in [Figure 1](#), strategies are being implemented worldwide to build a renewable energy economy and infrastructure<sup>[2]</sup>.

Solid oxide electrolytic cells (SOECs) are highly efficient electrolysis devices that convert water into hydrogen and oxygen through electrolysis. Compared with traditional low-temperature electrolysis technology, SOECs have higher energy efficiency and faster reaction rate, and show great potential in hydrogen production. However, the early experimental work usually focused on the synthesis and performance study of high-temperature solid oxide electrolytes. In recent years, with the worsening energy crisis and increasing environmental awareness, solid oxide electrolysis technology has received growing attention. Researchers have continuously improved the properties of solid oxide electrolytes, such as ionic conductivity, chemical stability and mechanical strength, by optimizing the material composition, microstructure and preparation process.

At present, solid oxide electrolysis cells (SOECs) play an important role in energy conversion, storage and utilization due to a number of advantages such as high-efficiency conversion, high-temperature operation and high-purity gas output. As most clean electricity is intermittent and variable and cannot be directly connected to the grid, SOECs can be used to convert electrical energy into chemical energy for long-term energy storage. Depending on the feed gas, SOECs can produce various products. H<sub>2</sub> can be produced by electrolysis of water, enabling large-scale production of “green hydrogen”. Compared with the conventional alkaline electrolysis, anion exchange membrane (AEM) and proton exchange membrane (PEM) hydrogen production technologies, SOECs are highly efficient, cost-effective and environmentally friendly. SOECs can also be used for the co-electrolysis of H<sub>2</sub>O and CO<sub>2</sub> to produce H<sub>2</sub>, CO and other chemical products<sup>[3]</sup>. Reversible solid oxide cells (RSOCs), which combine the advantages of both SOEC and solid oxide fuel cell (SOFC) models, play an important role in the carbon neutrality goal, as they enable carbon recycling in addition to promoting the efficient use of renewable energy sources and the production of “green hydrogen”<sup>[4]</sup>. RSOCs offer an efficient and sustainable solution to China's carbon neutrality goals and will play an important role in the world's energy system. [Table 1](#) shows the performance of different electrolysis technologies.

The higher temperatures required for SOEC systems reduce the demands on reaction kinetics, helping to overcome some limitations of conventional electrolysis cells. This results in increased electrolysis efficiency and reduced polarization losses. However, SOEC systems also face numerous challenges, including the disruption of material structure at high temperatures, expansion and contraction due to mismatched thermal expansion between the electrode material and other components during redox cycling, and the potential adverse effects of gases and other products generated during electrolysis on the electrode material<sup>[6]</sup>.

## WORKING PRINCIPLE OF SOEC

### Basic chemical reactions

SOECs are highly efficient electrochemical devices based on the conduction of oxygen ions or protons in solid oxide electrolytes. A SOEC consists essentially of a cathode (fuel electrode), an anode (air electrode) and a porous dense electrolyte (ion conductor) [[Figure 2](#)]. For a SOEC with oxygen ions conducting electrolyte, at high temperatures (typically between 600 and 1,000 °C), steam accepts electrons at the cathode and is reduced to form H<sub>2</sub> and O<sup>2-</sup>. At the same time, oxygen ions pass through a dense electrolyte

**Table 1. Technical characteristics of different water electrolysis technologies<sup>[5]</sup>**

	Alkaline water electrolysis	AEM	PEM	SOEC
Electrolyte	KOH/NaOH (1M)	KOH/NaOH (1M)	Solid polymer electrolyte	Solid oxide
Operating temperature (°C)	70-90	40-60	50-80	700-850
Nominal current density (A·cm <sup>-2</sup> )	0.2-0.8	0.2-2	1-2	0.3-1
Voltage range (V)	1.4-3	1.4-2.0	1.4-2.5	1.0-1.5
Cell pressure (bar)	< 30	< 35	< 70	< 10
Efficiency	50%-78%	57%-59%	50%-83%	89% (laboratory)
Lifetime (thousand hours)	60	> 30	50-80	20
H <sub>2</sub> purity	99.5%-99.9998%	99.9%-99.9999%	99.9%-99.9999%	99.9%
Development	Mature	R & D	Commercialized	R & D
Capital costs estimate for large stacks, > 1 MW (USD/kW <sub>el</sub> )	270	-	400	> 2,000
Capital cost range estimate for the entire system, > 10 MW (USD/kW <sub>el</sub> )	500-1,000	-	700-1,400	-

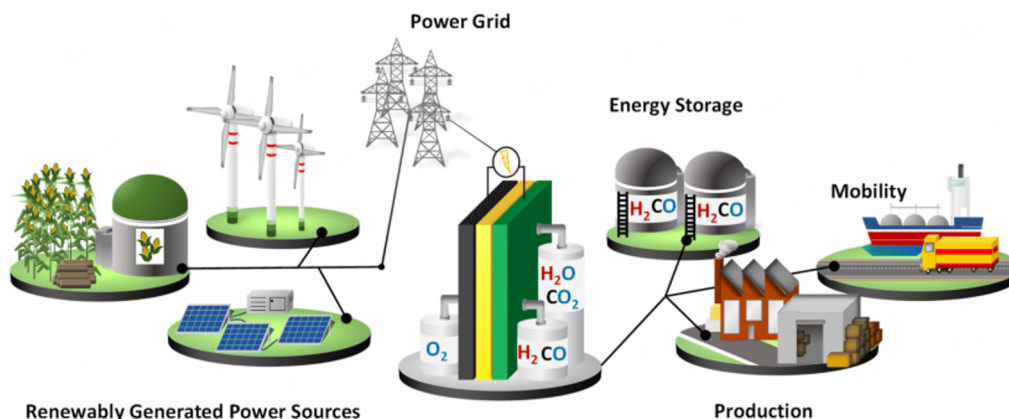


**Figure 1.** Schematic of clean energy applications. Reproduced with permission from Ref.<sup>[2]</sup>. Copyright 2023, The Royal Society of Chemistry.

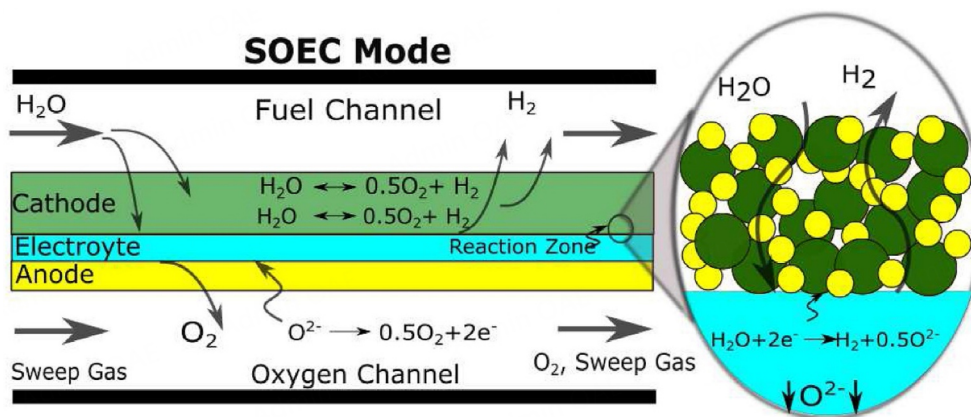


**Figure 2.** Working principle of SOECs. Reproduced with permission from Ref.<sup>[6]</sup>. Copyright 2023, Elsevier.

[usually yttria-stabilized zirconia (YSZ)] and are oxidized to oxygen. During electrolysis of H<sub>2</sub>O, CO<sub>2</sub> or both of them, the basic chemical reactions can be divided into two half-reactions, one at the cathode and another at the anode:

At the cathode side:



At the anode side:



## CATHODE

Cathodes, also known as fuel electrodes, provide active sites for the decomposition of H<sub>2</sub>O and transport channels for oxygen ions and gases, so they must have good electronic conductivity and catalytic activity to improve the efficiency of the electrolytic cells. Meanwhile, they generally have a loose porous structure to ensure the flow of gases. Since the reaction usually occurs at the triple phase boundaries (TPBs), the cathode must have high mixed ion-electron conductivity to extend the TPB area. However, long-term stability issues, such as particle aggregation, carbon deposition, nickel oxidation and sulfur poisoning, hinder further applications<sup>[7,8]</sup>.

### Cermet

Cermet materials are commonly used as cathodes. Pure metals have the disadvantages of mismatched thermal expansion coefficients, poor chemical stability, high-temperature creep, and high cost, making them unsuitable for direct use as SOEC cathodes<sup>[9]</sup>. By compositing with metals and ceramics, the advantages of both can be combined: excellent electronic conductivity and mechanical strength of metals, and good high-temperature stability and electrochemical properties of ceramics.

Ni-Y<sub>0.08</sub>Zr<sub>0.92</sub>O<sub>2+δ</sub> (Ni-YSZ) has excellent electrocatalytic activity, stability, and low preparation cost, and has been successfully commercialized in large-scale applications<sup>[10]</sup>. Ni, YSZ and pores can be used as transport channels for electrons, ions and gases. However, Ni particles tend to aggregate at high temperatures. In addition, problems such as carbon deposition, Ni oxidation and sulfur poisoning will further limit their application<sup>[11]</sup>.

Recent studies have shown that carbon atoms on the surface of cerium oxide-based materials such as Sm<sub>0.2</sub>Ce<sub>0.8</sub>O<sub>2-δ</sub> (SDC) and Ni-SDC can be trapped as carbon oxide intermediates, mitigating carbon deposition during CO<sub>2</sub> electrolysis [Figure 3]. Therefore, as SOEC cathodes, ceria or ceria-based materials can be further investigated.

Compared with Ni-based cermet materials, Cu-based materials have higher electronic conductivity and are less prone to carbon deposition. However, the catalytic activity of Cu is low, and the composite with metallic oxides that have higher catalytic activity is an effective method<sup>[13]</sup>.

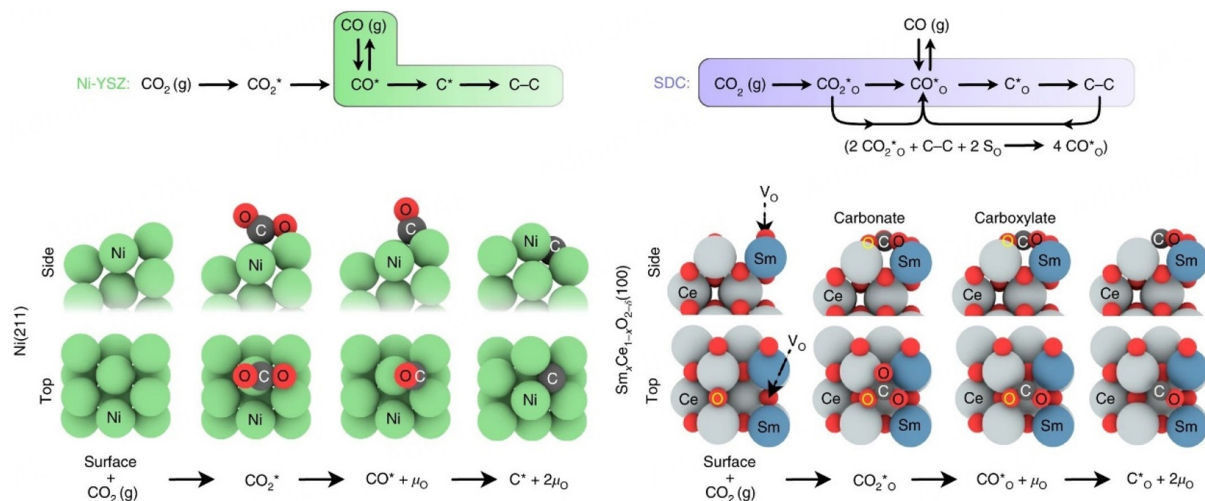


**Figure 3.** Mechanism of carbon formation on Ni and Ce surfaces. Reproduced with permission from Ref.<sup>[12]</sup>. Copyright 2018, Springer Nature.

In addition to Ni and Cu, other metal-doped cermetes can be used as SOEC cathodes. Ag has high electronic conductivity and chemical stability<sup>[14]</sup>. Compared to precious metals, Fe is cheaper, but it is easily oxidized at high temperatures. The alloy represents a significant avenue for enhancing the performance of electrode materials. The prevailing approach entails the uniform attachment of nano-alloy particles to the oxide surface, achieved through the *in situ* exsolution or impregnation techniques<sup>[15]</sup>. In a recent study, Wang *et al.* prepared Ni-M (M=Fe, Pt, Co, Cu, Ru) cathodes, respectively, and observed that the addition of Pt and Co resulted in a decrease in current density, whereas the addition of Fe, Cu, and Ru led to an improvement in electrode performance<sup>[16]</sup>. Among the alloys, the Ni-Fe alloy exhibited the most favorable performance. The main reason for this result is that Fe can effectively inhibit the agglomeration of Ni particles and the coking, thereby enhancing the stability of materials. Accordingly, the current research will focus on determining the optimal ratio of doping elements to enhance the promotion of dopants on electrode performance.

In conclusion, the implementation of diverse metal or alloy doping materials can enhance the electrochemical performance and catalytic activity of cathodes. However, the performance of other cermetes is still difficult to compare with that of Ni-based materials, and future research is needed to address the issues of stability and degradation in long-term operation. Table 2 presents a comparative analysis of the electrochemical performance of various cermetes. Among them, the performance of Ni-based materials is significantly superior to that of other metal element doping.

### Perovskite oxide-based materials

Compared to traditional cermet electrodes, perovskite oxides exhibit superior mixed ionic-electronic conductivity (MIEC), resistance to carbon deposition, and high-temperature stability<sup>[23]</sup>. Figure 4 depicts the structural configurations of single perovskites ( $\text{ABO}_3$ ) and double perovskites ( $\text{A}'\text{AB}'\text{BO}_6$ ).

The MIEC of perovskites enables the reaction to occur not only at the TPBs, but also at the gas-solid interface. This effectively reduces the polarization resistance. However, the lower catalytic activity of perovskite oxides greatly limits their applications. The A, B, and O sites in the perovskite structure can introduce various ions<sup>[24]</sup>. The use of doping, impregnation to introduce nano-catalysts, and *in-situ* exsolution can facilitate the formation of lattice defect structures and increase the concentration of oxygen

**Table 2. Electrochemical properties of different cermet**

Components	Conditions	Operating temperature/°C	Voltage/V	Current density/A·cm <sup>-2</sup>	Ref.
Ni-GDC	100% H <sub>2</sub> O	900	1.50	1.310	[17]
Ni-YSZ-BaCO <sub>3</sub>	70% CO <sub>2</sub> /CO	800	1.30	0.690	[18]
Ni-YSZ-Ni <sub>0.9</sub> Co <sub>0.1</sub> /SDC	100% H <sub>2</sub> O	800	0.07	0.500	[19]
Ni-SDC-Ni <sub>0.9</sub> Co <sub>0.1</sub> /SDC	100% H <sub>2</sub> O	800	1.21	0.500	[20]
Fe-SDC	95% CO <sub>2</sub> /N <sub>2</sub>	800	1.90	0.570	[21]
Cu-GDC	38% CO <sub>2</sub> /H <sub>2</sub>	750	2.00	0.071	[22]

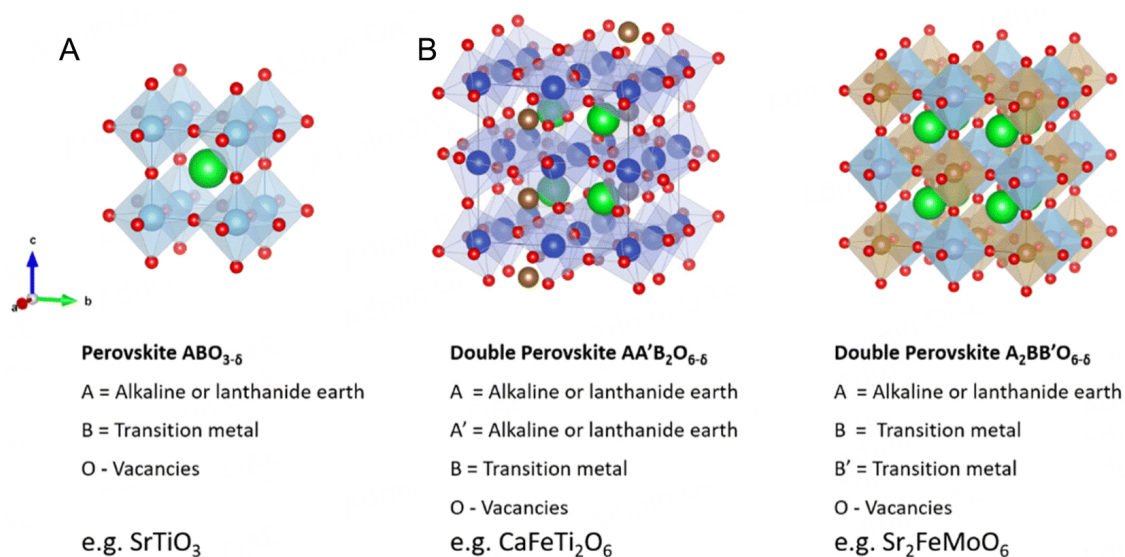


**Figure 4.** Structure of perovskite oxide materials. (A) The structure of single perovskite SrTiO<sub>3</sub>; (B) The structure of the double perovskite CaFeTi<sub>2</sub>O<sub>6</sub> and Sr<sub>2</sub>FeMoO<sub>6</sub>. Reproduced with permission from Ref. [2]. Copyright 2023, The Royal Society of Chemistry.

vacancies, thereby enhancing the catalytic ability of materials<sup>[25]</sup>. Moreover, the modification of surface nanostructures and the investigation of degradation mechanisms can also enhance material properties without altering the elemental composition<sup>[2]</sup>.

#### Single perovskites

Cr-based perovskites, exemplified by La<sub>0.75</sub>Sr<sub>0.25</sub>Cr<sub>0.5</sub>Mn<sub>0.5</sub>O<sub>3-δ</sub> (LSCM), are a prevalent class of single perovskites. It was demonstrated that the LSCM was capable of reaching a current density of 0.593 A·cm<sup>-2</sup> for the electrolysis of 80 vol.% H<sub>2</sub>O at 1.6 V and 850 °C, thereby exhibiting considerable potential as a fuel electrode for high-temperature steam electrolysis<sup>[26]</sup>. However, it still faces problems such as low electronic conductivity and poor catalytic activity. Ce doping can effectively improve the low conductivity of LSCM<sup>[27]</sup>, and the incorporation of metals, such as Ni and Fe, into the B-site of LSCM can markedly enhance its catalytic activity<sup>[28,29]</sup>.

SrFeO<sub>3-δ</sub> (SFO)-type perovskites exhibit excellent mixed ion-electron conductivity and catalytic activity. Nevertheless, the Fe<sup>4+</sup> in SFO can be readily reduced to Fe<sup>3+</sup> during electrolysis, which results in the decomposition of materials and renders it unsuitable for direct use in SOEC cathodes<sup>[30]</sup>. The doping of SFO with metal ions, such as La, Sc, Ni, Co, Mn and Nb, at the A or B sites is a common method of enhancing the stability of materials<sup>[31,32]</sup>. La<sub>0.7</sub>Sr<sub>0.3</sub>VO<sub>3</sub> (LSV)-based perovskites are suitable cathodes for SOECs, exhibiting excellent high-temperature stability and high conductivity under hydrogen and methane

conditions<sup>[33]</sup>. Nevertheless, the poor catalytic performance and harsh synthesis conditions restrict their further application. The impregnation of Ni or Fe nanoparticles onto the LSV surface can significantly improve its current density, and the ohmic resistance is almost unchanged, which is a promising method<sup>[34]</sup>.

SrTiO<sub>3-δ</sub> (STO)-based perovskites represent a class of materials that have been the subject of considerable research interest. The most widely used composition is 20% La-doped La<sub>0.2</sub>Sr<sub>0.8</sub>TiO<sub>3-δ</sub> (LST) at the A-site. In air, LST exhibits p-type conductivity, whereas in reducing atmospheres, it exhibits n-type conductivity<sup>[35]</sup>. LST demonstrates excellent stability under high-temperature reducing conditions and resistance to carbon accumulation, making it suitable for CO<sub>2</sub> electrolysis. However, its relatively low catalytic activity and oxygen ionic conductivity present obstacles to its broader application. Loading with nanometallic particles is an effective way to improve the catalytic performance<sup>[36]</sup>.

In addition to LST, Nb-doped STO (STN) materials are also widely used. The catalytic activity and cycling stability of STN can be enhanced through the doping of Nb elements at the B-site. Nevertheless, its direct application in steam electrolysis will encounter the challenge of inadequate catalytic efficacy. Yang *et al.* prepared (Sr<sub>0.94</sub>)<sub>0.9</sub>(Ti<sub>0.9</sub>Nb<sub>0.1</sub>)<sub>0.9</sub>Ni<sub>0.1</sub>O<sub>3</sub> (STNNO) cathodes with A-site defects and B-site excess by loading Ni nanoparticles on the STN surface<sup>[37]</sup>. It was demonstrated that the exsolution of Ni particles on the STN surface during the redox process was entirely reversible.

#### *Double perovskites*

The crystal structure of double perovskites comprises two mutually stacked metal hexahedral layers, where the metal elements are in disparate oxidation states. This configuration can offer active sites for electrolysis, and enhance the electrical conductivity. The presence of metal ions in two oxidation states within the structure results in a more complex oxygen ion conduction channel, thereby enabling precise regulation of the oxygen ion conduction properties<sup>[8]</sup>.

Sr<sub>2</sub>Fe<sub>1.5</sub>Mo<sub>0.5</sub>O<sub>6-δ</sub> (SFM) is a kind of prevalent double perovskite, which is an optimal SOEC cathode material due to its remarkable stability under redox conditions, favorable coefficient of thermal expansion, and high MIEC<sup>[38]</sup>. The performance of SFM can be enhanced by optimizing the ratio of Fe/Mo<sup>[39]</sup>. The oxidation ability increases with Fe content, which further enhances the hybridization of metal and oxygen, bringing the O 2p energy band closer to the Fermi energy level, thus increasing the concentration of oxygen vacancies and improving the catalytic activity of the material. Moreover, doping with elements such as Nb<sup>[40]</sup>, Zr<sup>[41]</sup>, Ba<sup>[42]</sup>, and others is also worth studying.

In addition to A and B-site doping, anionic doping of oxygen vacancies is also a viable approach. F-doping improves the adsorption capacity of CO<sub>2</sub> and the volumetric oxygen vacancy concentration, reduces polarization resistance, and accelerates the chemical reaction rate and the surface diffusion rate. The perovskite oxyfluoride compound, Sr<sub>2</sub>Fe<sub>1.5</sub>Mo<sub>0.5</sub>O<sub>6-δ</sub>F<sub>0.1</sub> (F-SFM), has a lower polarization resistance than that of SFM<sup>[43]</sup>.

The Mn-O-Mn lattice, formed by Mn ions of different valence states in PrBaMn<sub>2</sub>O<sub>5+δ</sub> (PBM)-based perovskites, facilitates the transport of oxygen ions and electrons, exhibits excellent carbon resistant properties, and demonstrates considerable potential as an electrolytic CO<sub>2</sub> cathode material<sup>[44]</sup>. The doping of PrBaFe<sub>2</sub>O<sub>5+δ</sub> (PBF) with Co has been demonstrated to enhance the electrochemical performance. PrBaFe<sub>1.8</sub>Co<sub>0.2</sub>O<sub>5+δ</sub> (PBFC02) is susceptible to decomposition during the reaction. However, it can be restored to its original structure through air calcination. Additionally, its favorable redox properties were highlighted. The electrochemical performance of PBFC02 was evaluated, and it was determined that the

material exhibited excellent performance in co-electrolysis of H<sub>2</sub>O/CO<sub>2</sub>, establishing it as an ideal candidate for the SOEC cathode<sup>[45]</sup>.

Overall, perovskites have attracted considerable attention due to their excellent mixed ion-electron conductivity and carbon-resistant properties. However, their conductivity is not as optimal as that of cermet cathodes. Although cermet materials have higher electronic conductivity and catalytic activity, they have problems such as easy migration and oxidation of metal elements at high temperatures. The development of more stable cathode materials remains a pivotal objective within the current research landscape. Furthermore, the study of the hydrogen electrode reaction mechanism and degradation mechanism is also a very interesting topic. *In-situ* investigations employing a range of advanced characterization tools, including transmission electron microscopy and X-ray photoelectron spectroscopy, when combined with first-principle calculations and model simulations, will facilitate the elucidation of the SOEC cathode reaction mechanism, and then find a way to improve the electrochemical performance of the cathode material. In order to visualize the electrochemical properties of different perovskite cathode materials, the performance differences between them are given in [Table 3](#).

## ANODE

Oxygen evolution reaction (OER) occurs at anodes of SOECs. Consequently, the anodes must exhibit high electronic conductivity, ionic conductivity, catalytic activity, appropriate redox activity, and a matched thermal expansion coefficient with electrolytes. The reaction typically involves the diffusion of oxygen; it is necessary for anode to have a porous microstructure. Nevertheless, the issue of electrode and electrolyte delamination during prolonged operation represents the most significant obstacle to the advancement of SOEC anodes. To enhance stability, current research is mainly focused on the development of advanced materials and microstructures and the optimization of existing techniques<sup>[63]</sup>.

### Materials design

La<sub>1-x</sub>Sr<sub>x</sub>MnO<sub>3-δ</sub> (LSM) has high catalytic activity and electronic conductivity, along with a matched coefficient of thermal expansion and favorable chemical compatibility with YSZ electrolyte materials<sup>[64]</sup>. It has been demonstrated that LSM will form a localized region of elevated oxygen partial pressure during long-term operation. This will result in delamination with the electrolyte interface, thereby increasing the resistance of the electrode and potentially leading to a decay of the performance of SOEC or even its failure<sup>[65]</sup>. Su *et al.* employed the spin-coating method to create a porous layer of YSZ between the LSM and the electrolyte [[Figure 5A](#)]<sup>[66]</sup>. It was found that the introduction of the YSZ porous layer accelerated the diffusion of oxygen ions at the solid-solid two-phase interface (SSTPI), which led to a reduction in the oxygen partial pressure in the SSTPI zone and inhibited the degradation of the anode. Furthermore, the TPB area was increased, thereby improving the performance of SOECs. The reversible cycle operation serves to decelerate the kinetic rate of the OER at the anode.

The doping of A-site rare earth or alkaline-earth metal ions is another common method for increasing the concentration of oxygen vacancies, which is used to enhance the performance of anodes. As shown in [Figure 5B](#) and [C](#), the introduction of Au nanoparticles onto LSM-YSZ by impregnation can accelerate the electron transfer rate and the formation of new TPBs during the reaction, thereby enhancing the stability of the anode in an atmosphere with a higher oxygen partial pressure<sup>[67]</sup>. Mahata *et al.* prepared LSCM with Sr substituted by Ca by combustion synthesis and found that the electronic conductivity of the final product varies with the Ca content<sup>[68]</sup>. When Sr was completely replaced by Ca, the electronic conductivity of LCM increased with the Ca percentage; while Sr was partially replaced, the conductivity decreased with the increasing Ca percentage. As illustrated in [Figure 5D](#), the hydrogen production of LCM is markedly higher than pure LSM and partially Ca-doped LSCM. Furthermore, the hydrogen production does not decrease

**Table 3. Electrochemical properties of common perovskite cathode materials**

Components	Conditions	Operating temperature/°C	Volt./V	Current density/A·cm <sup>-2</sup>	Ref.
La <sub>0.75</sub> Sr <sub>0.25</sub> Cr <sub>0.5</sub> Mn <sub>0.5</sub> O <sub>3-δ</sub>	5% H <sub>2</sub> O/5% H <sub>2</sub> /Ar	800	1.00	0.5528	[46]
La <sub>0.65</sub> Sr <sub>0.3</sub> Cr <sub>0.85</sub> Ni <sub>0.15</sub> O <sub>3-δ</sub>	80% H <sub>2</sub> O/H <sub>2</sub>	830	1.29	0.650	[46]
Fe-La <sub>0.75</sub> Sr <sub>0.25</sub> Cr <sub>0.5</sub> Mn <sub>0.5</sub> O <sub>3-δ</sub>	3% H <sub>2</sub> O/5% H <sub>2</sub> /Ar	800	2.00	0.110	[47]
(La <sub>0.75</sub> Sr <sub>0.25</sub> ) <sub>0.95</sub> (Cr <sub>0.8</sub> Ni <sub>0.2</sub> ) <sub>0.95</sub> Ni <sub>0.05</sub> O <sub>3-δ</sub>	3% H <sub>2</sub> O/5% H <sub>2</sub> /Ar	800	2.00	0.093	[48]
(La <sub>0.2</sub> Sr <sub>0.8</sub> ) <sub>0.9</sub> Ti <sub>0.5</sub> Mn <sub>0.4</sub> Cu <sub>0.1</sub> O <sub>3-δ</sub>	100% CO <sub>2</sub>	800	1.80	2.820	[49]
-La <sub>0.8</sub> Sr <sub>0.2</sub> FeO <sub>3</sub>	20% H <sub>2</sub> O/20% H <sub>2</sub> /Ar	800	1.40	0.920	[50]
(La <sub>0.65</sub> Sr <sub>0.3</sub> Ce <sub>0.05</sub> ) <sub>0.9</sub> (Cr <sub>0.5</sub> Fe <sub>0.5</sub> ) <sub>0.8</sub> Ni <sub>0.15</sub> O <sub>3-δ</sub>	100% CO <sub>2</sub>	850	1.85	2.260	[24]
La <sub>0.6</sub> Ca <sub>0.4</sub> Fe <sub>0.8</sub> Ni <sub>0.2</sub> O <sub>3-δ</sub>	100% CO <sub>2</sub>	800	2.00	1.500	[51]
La <sub>1.2</sub> Sr <sub>0.8</sub> Mn <sub>0.4</sub> Fe <sub>0.6</sub> O <sub>4-δ</sub>	70% CO <sub>2</sub> /CO	850	1.50	2.040	[52]
PrBaMn <sub>2</sub> O <sub>5+δ</sub>	70% CO <sub>2</sub> /CO	850	1.50	0.850	[53]
Pr <sub>0.3</sub> Sr <sub>0.7</sub> Ti <sub>0.3</sub> Fe <sub>0.7</sub> O <sub>3-δ</sub>	60% H <sub>2</sub> O/H <sub>2</sub> /Ar	800	1.46	0.302	[54]
Pr <sub>0.4</sub> Sr <sub>0.6</sub> Co <sub>0.2</sub> Fe <sub>0.7</sub> Mo <sub>0.1</sub> O <sub>3-δ</sub>	70% CO <sub>2</sub> /CO	850	1.60	1.010	[55]
Pr <sub>0.4</sub> Sr <sub>1.6</sub> (NiFe) <sub>1.5</sub> Mo <sub>0.5</sub> O <sub>6-δ</sub>	100% CO <sub>2</sub>	800	1.40	1.580	[56]
Sm <sub>0.9</sub> Ca <sub>0.1</sub> Fe <sub>0.9</sub> Cu <sub>0.1</sub> O <sub>3-δ</sub>	100% CO <sub>2</sub>	800	1.50	1.200	[57]
Sr <sub>0.95</sub> Ti <sub>0.8</sub> Nb <sub>0.1</sub> Mn <sub>0.1</sub> O <sub>3</sub>	100% CO <sub>2</sub>	800	2.00	0.348	[58]
Sr <sub>0.95</sub> (Ti <sub>0.3</sub> Fe <sub>0.63</sub> Ru <sub>0.07</sub> )O <sub>3-δ</sub>	50% H <sub>2</sub> O/H <sub>2</sub>	800	1.30	1.700	[59]
SF <sub>1.575</sub> M-SDC	100% CO <sub>2</sub>	850	1.60	0.750	[60]
Sr <sub>2</sub> Fe <sub>1.3</sub> Zr <sub>0.2</sub> Mo <sub>0.5</sub> O <sub>6-δ</sub>	100% CO <sub>2</sub>	800	1.80	1.850	[41]
Sr <sub>2</sub> Fe <sub>1.5</sub> Mo <sub>0.3</sub> Cu <sub>0.2</sub> O <sub>6-δ</sub>	100% CO <sub>2</sub>	800	1.40	1.940	[61]
Co-Fe-Sr <sub>2</sub> Ti <sub>0.8</sub> Co <sub>0.2</sub> FeO <sub>6-δ</sub>	100% CO <sub>2</sub>	800	1.60	1.260	[62]

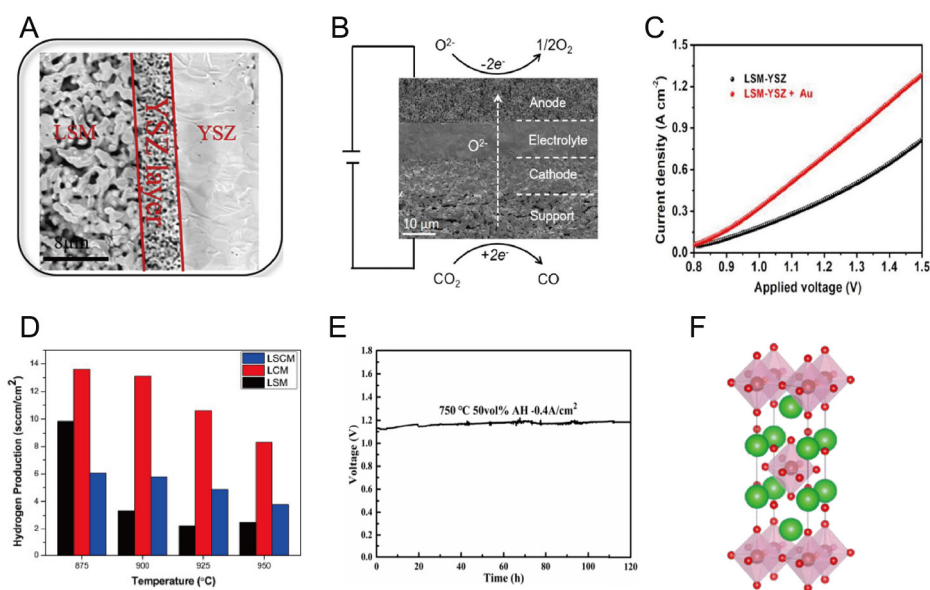


**Figure 5.** (A) Cross-sectional scanning electron microscopy (SEM) images of the LSM with YSZ. Reproduced with permission from Ref. [66]. Copyright 2019, Elsevier. (B) Cross-sectional SEM images of the SOEC. Reproduced with permission from Ref. [67]. Copyright 2019, Elsevier. (C) *I*-*V* curves of the LSM-YSZ and Au-LSM-YSZ. Reproduced with permission from Ref. [67]. Copyright 2019, Elsevier. (D) Hydrogen production of the LSM, LCM, and LSCM at different temperatures. Reproduced with permission from Ref. [68]. Copyright 2017, Elsevier. (E) Constant current stability test in SOEC mode. Reproduced with permission from Ref. [69]. Copyright 2018, Elsevier. (F) Schematic representation of the Ruddlesden-Popper-type perovskite structure. Reproduced with permission from Ref. [2]. Copyright 2023, The Royal Society of Chemistry.

significantly with increasing temperature, suggesting the potential of LCM as an anode material for SOECs.

In addition to LSM, B-site transition metal ion ( $\text{Fe}^{3+}$ ,  $\text{Co}^{3+}$ , and  $\text{Ni}^{3+}$ )-doped perovskites have also been demonstrated to enhance the oxygen vacancy concentration. Among them, Co and Fe co-doped  $\text{La}_{1-x}\text{Sr}_x\text{Co}_{1-y}\text{Fe}_y\text{O}_{3-\delta}$  has been the subject of considerable research interest due to its stability and catalytic activity in OER. A discontinuous Sr layer was formed between LSCF and YSZ during anode polarization. This inhibited the segregation of Sr and the movement toward the electrode/electrolyte interface, resulting in the formation of a stable electrode/electrolyte layer. This greatly improves the performance of SOECs. Furthermore, doping other metal elements has also been demonstrated to enhance the performance of LSCF-based oxygen electrodes. Tian *et al.* synthesized  $\text{PrBa}_{0.5}\text{Sr}_{0.5}\text{Co}_{1.5}\text{Fe}_{0.5}\text{O}_{5+\delta}$  (PBSCF) double-perovskite by wet-chemical method, and then electrolyzed at 850 °C, 2.0 V, and 70 vol% absolute humidity<sup>[69]</sup>. Results showed a hydrogen production rate of up to 1,544 mL·cm<sup>-2</sup>·h<sup>-1</sup>, with a maximum current density of 3.694 A·cm<sup>-2</sup>. Additionally, the material demonstrated high stability, as shown in Figure 5E. Among them, the excellent performance of PBSCF under polarized conditions may be due to its high intrinsic catalytic activity, which proves that SOECs based on this type of material have a wide range of applications.

Ruddlesden-Popper (R-P)-phase perovskites have the structure  $\text{A}_{n+1}\text{B}_n\text{O}_{3n+1}$ . As shown in Figure 5F, this type has an alternating structure of AO rock salt lattice and perovskites, and generally exhibits high oxygen mobility and stability. The typical R-P-phase perovskites are  $\text{Ln}_2\text{NiO}_{4+\delta}$  (LNO) and  $\text{Pr}_2\text{NiO}_{4+\delta}$  (PNO)-based materials, which can accommodate more oxygen, have lower polarization resistance, and exhibit excellent oxygen transport properties. Additionally, they are free of Sr and Co, which can avoid being poisoned by cobalt in the reactant gas and have good chemical stability<sup>[70]</sup>. In order to gain insight into the mechanism of oxygen transport in R-P perovskites, Gu *et al.* conducted an in-depth analysis of 20 samples comprising six distinct R-P perovskites, such as  $\text{La}_2\text{NiO}_4$ ,  $\text{La}_2\text{CoO}_4$ , *etc.*<sup>[71]</sup>. Their findings revealed that the OER during the anodic electrolysis process is influenced by three key factors: the interstitial oxygen ion concentration, the migration of interstitial oxygen ions, and the migration of lattice oxygen. Therefore, they believe that the doping of metal ions in a reasonable quantity can be employed to enhance the material properties and accelerate the reaction rate. Therefore, future research should focus on the optimization of such materials and the study of reaction mechanisms.

At present, the majority of SOEC anodes are perovskites containing Sr and Co, which face the problems of Sr segregation and Co poisoning. Consequently, Co- and Sr-free R-P perovskites have been gradually gaining prominence, yet their utilization in SOECs has durability challenges. Consequently, experimental confirmation of the crystal structure and physicochemical attributes of the samples remains a necessity. Hence, the current research should focus on understanding the reaction mechanism, optimizing electrode properties, developing new materials or improving existing ones, and making a reasonable choice between catalytic activity and stability. Table 4 provides a brief summary of the anode materials and their electrolytic cell properties from selected studies on SOEC anodes in recent years. It can be seen that elemental doping is still the main means to improve the performance of anode materials.

### Microstructure modification

In addition to the design of new materials, the appropriate adjustment of the microstructure of existing materials is also a useful approach to improving the performance of materials. By precisely adjusting the microstructure (i.e., porosity, pore size, and distribution), the area of TPBs can be increased to ensure sufficient active surface area during the reaction, which can reduce polarization loss. Nevertheless, the porosity must be constrained to a specific range, as excessive porosity will impair the stability of the electrodes and diminish the TPB area<sup>[91]</sup>.

**Table 4. SOEC anodes and cell performance in recent literature**

Components	Conditions	Operating temperature/°C	Volt./V	Current density/A·cm <sup>-2</sup>	Ref.
LSM	50% H <sub>2</sub> O/H <sub>2</sub>	900	0.70	0.500	[72]
LSM-SDC-CuO	40 vol% RH	800	1.50	0.360	[73]
LSM-YSZ-SrTi <sub>0.3</sub> Fe <sub>0.6</sub> Co <sub>0.1</sub> O <sub>3-δ</sub>	50% H <sub>2</sub> O/H <sub>2</sub>	800	1.30	2.000	[74]
Y-stabilized Bi <sub>2</sub> O <sub>3</sub> -LSM	45% AH	800	1.28	1.520	[75]
La <sub>0.6</sub> Sr <sub>0.4</sub> Fe <sub>0.9</sub> Mn <sub>0.1</sub> O <sub>3-δ</sub>	100% CO <sub>2</sub>	850	2.00	1.744	[76]
La <sub>0.6</sub> Sr <sub>0.4</sub> FeO <sub>3-δ</sub> -YSZ	50% H <sub>2</sub> O/25% H <sub>2</sub> /N <sub>2</sub>	800	1.30	0.660	[77]
LSCF	63% H <sub>2</sub> O/7% H <sub>2</sub> /N <sub>2</sub>	900	1.30	0.780	[78]
LSCF-GDC	80% H <sub>2</sub> O/H <sub>2</sub>	773	1.20	0.750	[79]
La <sub>0.4</sub> Sr <sub>0.6</sub> Co <sub>0.2</sub> Fe <sub>0.7</sub> Nb <sub>0.1</sub> O <sub>3-δ</sub>	75% CO <sub>2</sub> /15% H <sub>2</sub> O/H <sub>2</sub>	850	1.30	0.638	[80]
La <sub>0.3</sub> Sr <sub>0.7</sub> Fe <sub>0.7</sub> Ti <sub>0.3</sub> O <sub>3</sub>	100% CO <sub>2</sub>	800	2.00	0.521	[81]
Ba <sub>0.6</sub> Sr <sub>0.4</sub> Co <sub>0.8</sub> Fe <sub>0.2</sub> O <sub>3</sub>	50% H <sub>2</sub> O/H <sub>2</sub>	800	1.30	1.370	[82]
SrCo <sub>0.8</sub> Fe <sub>0.1</sub> Ga <sub>0.1</sub> O <sub>3-δ</sub>	40% AH	850	1.50	2.221	[83]
BaZr <sub>0.2</sub> Co <sub>0.8</sub> O <sub>3-δ</sub>	50% H <sub>2</sub> O/H <sub>2</sub>	800	1.30	1.430	[84]
CaMn <sub>0.9</sub> Nb <sub>0.1</sub> O <sub>3-δ</sub>	50% H <sub>2</sub> O/3% H <sub>2</sub> /N <sub>2</sub>	700	1.70	0.210	[85]
SFM-YSZ	75% H <sub>2</sub> O/H <sub>2</sub>	750	1.20	0.327	[86]
La <sub>2</sub> NiO <sub>4+δ</sub>	21% H <sub>2</sub> O/N <sub>2</sub>	750	0.107	0.500	[87]
PrBaCo <sub>2</sub> O <sub>5+δ</sub>	90% CO <sub>2</sub> /CO	750	1.30	0.750	[88]
Nd <sub>1.95</sub> Ba <sub>0.05</sub> NiO <sub>4+δ</sub>	pH <sub>2</sub> O = 0.03 atm	750	1.60	1.210	[89]
Pr <sub>2</sub> NiO <sub>4+δ</sub>	50% H <sub>2</sub> O/H <sub>2</sub>	800	1.20	0.980	[90]
PrBaFe <sub>1.8</sub> Co <sub>0.2</sub> O <sub>5+δ</sub>	50% H <sub>2</sub> O/CO <sub>2</sub>	850	1.30	0.650	[45]

The conventional preparation processes make it difficult to obtain pores of appropriate size and uniform distribution. Wu *et al.* developed a novel anode with a biomimetic honeycomb structure using freeze-casting and infiltration techniques<sup>[92]</sup>. The material was found to have a porosity of approximately 75%, an ultra-high-strength three-dimensional structure, and an ultra-low polarization resistance of 0.0094 Ω·cm<sup>2</sup>. The honeycomb structure facilitates the rapid diffusion of oxygen and accelerates the mobility of electrons and ions. Nanocomposites are also widely used in improving the performance of the anodes. In addition, designing the skeleton structure for easy gas flow is also a method to improve the performance of SOECs. Cao *et al.* employed La<sub>0.6</sub>Sr<sub>0.4</sub>CoO<sub>3-δ</sub> as an anode catalytic nanolayer and designed a vertically aligned backbone structure to promote the oxygen generation and release rate<sup>[93]</sup>. Additionally, they integrated the electrode/electrolyte interface to avoid delamination. Furthermore, the performance of anodes can be enhanced by preparing the nanocomposite materials, constructing the new interface, and developing alternative synthesis methods, e.g., pulsed laser deposition or magnetron sputtering.

## ELECTROLYTE

Electrolytes represent the fundamental component of SOECs, responsible for facilitating ion conduction while separating reducing and oxidizing gases at the two electrodes. Consequently, they must exhibit high ionic conductivity, compatibility with electrodes, matched thermal expansion coefficients and sufficient mechanical strength<sup>[94]</sup>. As shown in Figure 6A and B, SOECs can be classified into two categories: oxygen-ion conductor SOECs (O-SOECs) and proton conductor SOECs (H-SOECs), based on the conducting ions present in the electrolyte.

### Electrolytes of O-SOECs

During electrolysis, oxygen ions migrate from the cathode to the anode via oxygen vacancies in the electrolyte. The conductivity is contingent upon the concentration of oxygen vacancies. It has been demonstrated that the ionic conductivity of the electrolytes will increase with temperatures. However,

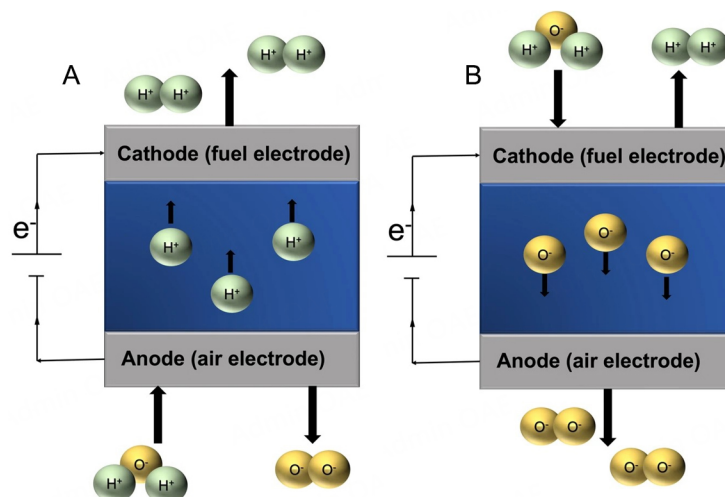


**Figure 6.** Schematic of SOECs for different types of electrolytes. (A) H-SOECs; (B) O-SOECs. Reproduced with permission from Ref.<sup>[95]</sup>. Copyright 2023, Springer Nature.

higher temperatures result in an increase in the difference in the coefficient of thermal expansion between the electrode and electrolyte<sup>[96]</sup>. The current research mainly focuses on lowering the reaction temperature, enhancing stability, and increasing the conductivity of oxygen ions<sup>[97]</sup>.

ZrO<sub>2</sub> has various crystal structures; depending on the temperatures, it transforms between different phases<sup>[98]</sup>. However, pure ZrO<sub>2</sub> is typically non-conducting and results in reduced stability during changes of crystal structure. Its ionic conductivity is significantly enhanced by doping with divalent or trivalent metal cations<sup>[99]</sup>. It was determined that the 8-10 mol% YSZ exhibited the optimal ionic transport properties<sup>[100]</sup>. However, YSZ exhibits a high polarization resistance below 700 °C, and thin-film techniques are typically employed to reduce its resistivity. The common methods include chemical vapor deposition<sup>[101]</sup>, film casting<sup>[102]</sup>, and screen printing<sup>[103]</sup> [Figure 7A].

Sc<sub>2</sub>O<sub>3</sub>-doped ZrO<sub>2</sub> (ScSZ) also exhibits suitable ionic conductivity and a thermally stable structure. At 780 °C, it reaches a conductivity of 0.14 S·cm<sup>-1</sup>, which is more suitable for low and medium temperatures than YSZ<sup>[104]</sup>. As the temperature decreases, the structure of ScSZ undergoes a transformation from cubic to tetragonal, which results in a reduction in the ionic conductivity and stability of ScSZ<sup>[105]</sup>. This issue can be addressed by co-doping other oxides. Bernadet *et al.* prepared a symmetric cell [Figure 7B] using (ZrO<sub>2</sub>)<sub>0.9</sub>(Yb<sub>2</sub>O<sub>3</sub>)<sub>0.06</sub>(Sc<sub>2</sub>O<sub>3</sub>)<sub>0.04</sub> (YbScSZ) as the electrolyte<sup>[106]</sup>. They observed that the current density for electrolysis of 90% H<sub>2</sub>O/Ar at 900 °C and 1.3 V up to 1.4 A·cm<sup>-2</sup>. Nevertheless, the elevated cost of Sc-based materials suggests that it may be challenging to substitute YSZ for commercial applications.

Pure CeO<sub>2</sub> exhibits a minimal capacity for conducting oxygen ions<sup>[107]</sup>. As illustrated in Figure 7C<sup>[108]</sup>, to enhance the ionic conductivity of CeO<sub>2</sub>, rare earth metal ions situated in close proximity to the Ce<sup>4+</sup> radius are typically employed for doping or co-doping. Among these, Gd<sub>2</sub>O<sub>3</sub>-doped CeO<sub>2</sub> (GDC) and SDC have been demonstrated to exhibit high oxygen ionic conductivity and excellent low and medium temperatures electrolytic properties<sup>[109]</sup>. However, Ce<sup>4+</sup> in the CeO<sub>2</sub>-based electrolyte is partially reduced to Ce<sup>3+</sup> during the reaction process, exhibiting MIEC. This results in localized short-circuiting, which has the effect of reducing the performance of SOECs<sup>[110]</sup>. To address this issue, Qian *et al.* employed BaMn<sub>1-x</sub>Ni<sub>x</sub>O<sub>3</sub> as an anode precursor to circumvent the internal short circuit of the cell and augment the open-circuit voltage by incorporating an electron-blocking layer (4 μm in thickness) predominantly comprising BaCeO<sub>3</sub> in the SDC-

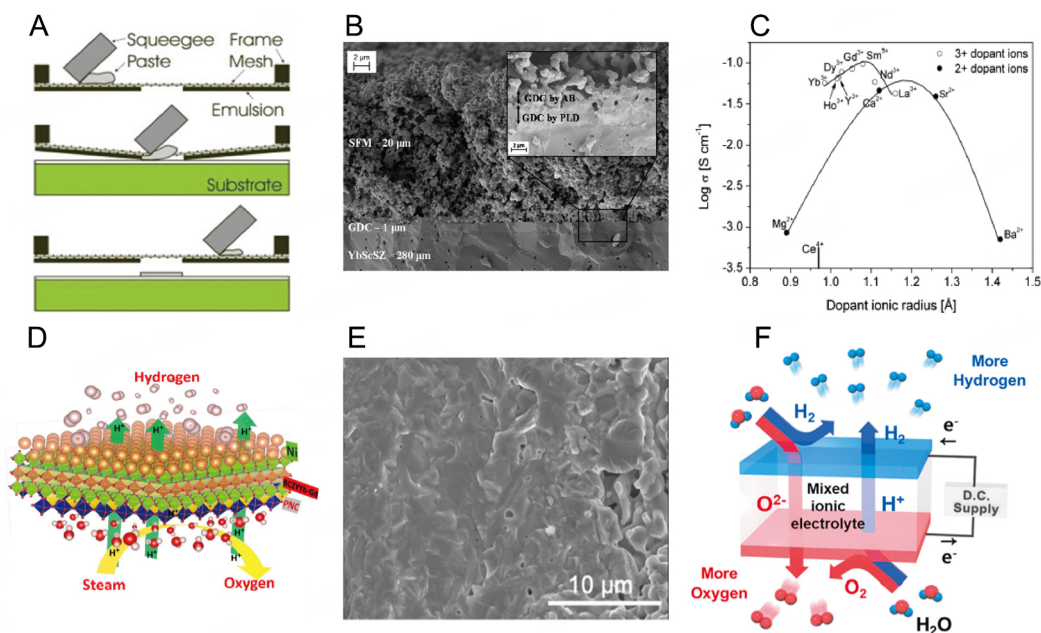


**Figure 7.** (A) Schematic of the screen-printing. Reproduced with permission from Ref. [103]. Copyright 2012, Elsevier. (B) SEM image of the cross-section of SOEC. Reproduced with permission from Ref. [106]. Copyright 2020, Elsevier. (C) Effect of ionic radius of different dopant elements on the ionic conductivity of CeO<sub>2</sub>-based electrolyte. Reproduced with permission from Ref. [108]. Copyright 2007, Elsevier. (D) Schematic of the constituent atoms of SOEC. Reproduced with permission from Ref. [118]. Copyright 2020, American Chemical Society. (E) SEM image of the dense BZCYb/LCO layer. Reproduced with permission from Ref. [119]. Copyright 2019, American Chemical Society. (F) Schematic of the working principle of the Hybrid-SOEC. Reproduced with permission from Ref. [120]. Copyright 2018, Elsevier.

based cell<sup>[111]</sup>. There are still some problems with CeO<sub>2</sub>-based electrolytes, and the addition of barrier layers and the selection of appropriate types and ratios of co-dopant elements will be the focus of future research.

LaGaO<sub>3</sub> is an oxygen ion conductor electrolyte with a perovskite structure, which exhibits superior ion-conducting capabilities and enhanced chemical stability at low and medium temperatures. The doping of LaGaO<sub>3</sub>-based electrolytes with alkaline earth or transition metal elements at the A-site and B-site, respectively, has been demonstrated to enhance performance. A series of LaGaO<sub>3</sub>-based electrolytes were studied by Ishihara *et al.*, who identified La<sub>1-x</sub>Sr<sub>x</sub>Ga<sub>1-y</sub>Mg<sub>y</sub>O<sub>3-δ</sub> (LSGM) as the electrolyte with the highest ionic conductivity<sup>[112]</sup>. Furthermore, they observed that as the La content increased and the Sr content decreased, the performance of LSGM was improved further<sup>[113]</sup>. However, the volatility of Ga elements under high-temperature reducing atmospheres presents significant challenges to the development of LSGM. The introduction of a buffer layer between the LSGM and the electrode material serves to avoid the chemical reaction between them. Tan *et al.* employed a dip-coating and co-sintering process to load Sm<sub>0.5</sub>Sr<sub>0.5</sub>CoO<sub>3-δ</sub> (SSC) into the LSGM layer<sup>[114]</sup>. The incorporation of a buffer layer was observed to diminish the cathode overpotential and augment the long-term stability of electrode materials. Despite the high ionic conductivity of perovskite electrolytes, they are hindered by two significant challenges: the high cost of production and the incompatibility of their thermal expansion coefficients with those of electrode materials.

In summary, the traditional oxygen ion conductor electrolyte materials are inadequate for the current requirements of low-temperature electrolysis. Additionally, there are also a series of issues, including material degradation and thermal expansion coefficient mismatch.

### Electrolytes of H-SOECs

The H-SOEC can operate at low temperatures ( $< 500\text{ }^{\circ}\text{C}$ ) due to the use of a proton conductor as the electrolyte<sup>[115]</sup>.  $\text{BaCeO}_3$  exhibits high proton conductivity and facile firing, but its diminished chemical stability in steam makes it unfeasible for direct utilization as a SOEC electrolyte<sup>[116]</sup>.  $\text{BaCe}_{0.8}\text{Y}_{0.2}\text{O}_{3-\delta}$  (BCY), prepared by Y doping, exhibits higher proton conductivity; however, it is not stable in the high concentration of  $\text{H}_2\text{O}$  and  $\text{CO}_2$  atmospheres. Yang *et al.* prepared  $\text{BaCe}_{0.7}\text{Zr}_{0.1}\text{Y}_{0.1}\text{Yb}_{0.1}\text{O}_3$  (BZCYYb) solid electrolyte using Yb doping<sup>[117]</sup>. Results showed that high ionic conductivity and chemical stability were archived at low temperatures ( $500\sim 700\text{ }^{\circ}\text{C}$ ), along with excellent resistance to sulfur and coking. As shown in Figure 7D and E, Gd doping<sup>[118]</sup> or adding a barrier layer at the electrolyte interface<sup>[119]</sup> can further improve the performance of SOECs.

In SOEC systems, simultaneous electrolytic oxidation of the reactants at both the cathode and anode can be achieved, resulting in an enhanced yield. Kim *et al.* prepared a hybrid SOEC (Hybrid-SOEC, Figure 7F) with  $\text{BaZr}_{0.1}\text{Ce}_{0.7}\text{Y}_{0.1}\text{Yb}_{0.1}\text{O}_{3-\delta}$  as an electrolyte<sup>[120]</sup>. The electrolysis of 10%  $\text{H}_2\text{O}/\text{H}_2$  at  $700\text{ }^{\circ}\text{C}$  and 1.3 V resulted in a current density of  $3.16\text{ A}\cdot\text{cm}^{-2}$ , which far exceeded that of the electrolyte material with a single conductor. Furthermore, the cell shows no significant performance degradation during more than 60 h of continuous operation. This means that it is a stable and efficient hydrogen production system. In conclusion, the conventional oxygen ion conductor electrolytes are not suitable for the current requirements for low-temperature electrolysis. The higher ionic conductivity of proton-conducting electrolytes at low temperatures aligns with the development trend of low- and medium-temperature SOCs, making further research in this area worthwhile. Hybrid-SOEC exhibits a high hydrogen production rate, but it remains in the laboratory stage of development. In order to accurately represent the performance differences between different electrolyte materials, the conductivities of various materials have been collated and are presented in Table 5.

### SOEC CONFIGURATIONS

It is essential that the SOECs have a stable structure to ensure the mechanical strength of the cell. As illustrated in Figure 8, the common SOECs can be classified into three distinct categories based on the type of support layer: fuel electrode-supported cells (FESCs), oxygen electrode-supported cells (OESCs), and electrolyte-supported cells (ESCs).

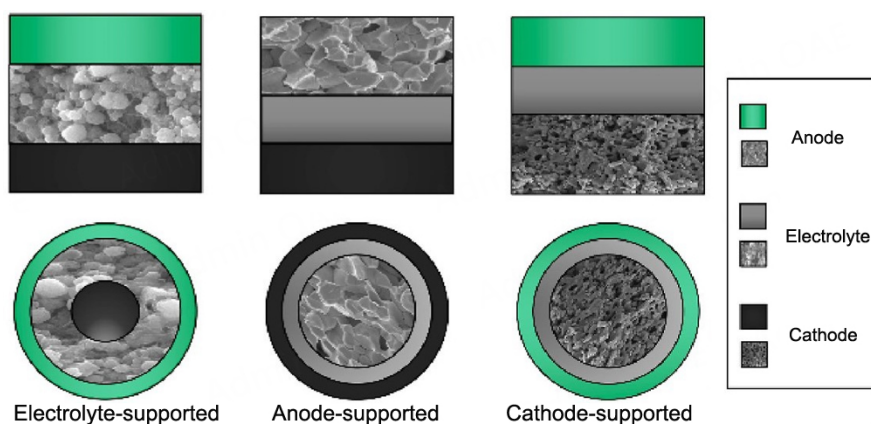
#### Electrode-supported cells

The resistance of SOECs is attributable to the ohmic resistance of the electrolytes and the polarization resistance of the electrodes. The utilization of fuel electrodes as the support layer can diminish the electrolyte thickness, thereby attenuating the impact of ohmic resistance on the electrolytic cell. However, the anode in FESCs is insufficiently thick, and the oxygen generated during the reaction increases the oxygen partial pressure at the anode/electrolyte interface, which causes delamination or fracture at the interface and significantly reduces the stability of SOECs<sup>[131]</sup>. The selection of an appropriate thickness ( $5\text{--}20\text{ }\mu\text{m}$ ) for the active electrode layer of the fuel electrode and the reduction of the electrolyte thickness can result in a reduction of ohmic resistance and operating temperature for the cells. Thus, it can lead to an enhancement in the electrochemical performance and redox stability of the FESCs<sup>[132]</sup>.

OESCs facilitate the reduction of electrolyte and cathode thickness, thereby diminishing the ohmic resistance of the electrolytic cell. Additionally, they prevent delamination caused by volume changes in the cathode material. However, conventional perovskites result in a reduction in anode pore structures during high-temperature sintering, which subsequently causes barriers for gas diffusion. The construction of asymmetric thick OESCs with a robust anode-electrolyte interface and dendritic anode gas diffusion

**Table 5. Comparison of properties of electrolyte materials**

Components	Operating temperature/°C	Conductivity/S cm <sup>-1</sup>	Ref.
8YSZ	1,000	0.140	[100]
ScSZ	850	0.178	[121]
Ce <sub>0.8</sub> Sm <sub>0.2</sub> O <sub>3-δ</sub>	800	0.100	[122]
1Bi10ScSZ	1,000	0.330	[123]
La <sub>0.9</sub> Sr <sub>0.1</sub> Ga <sub>0.8</sub> Mg <sub>0.2</sub> O <sub>2.85</sub>	800	0.110	[124]
La <sub>0.8</sub> Sr <sub>0.2-x</sub> Ba <sub>x</sub> Ga <sub>0.8</sub> Mg <sub>0.2</sub> O <sub>2.8</sub>	600	0.046	[125]
BaZr <sub>0.6</sub> Co <sub>0.4</sub> O <sub>3-δ</sub>	700	0.012	[126]
BaCe <sub>0.5</sub> Zr <sub>0.3</sub> Dy <sub>0.2</sub> O <sub>3-δ</sub>	600	0.019	[127]
BaCe <sub>0.5</sub> Zr <sub>0.2</sub> In <sub>0.3</sub> O <sub>3-δ</sub>	750	0.0064	[128]
BaCe <sub>0.68</sub> Zr <sub>0.1</sub> Y <sub>0.1</sub> Yb <sub>0.1</sub> Cu <sub>0.02</sub> O <sub>3-δ</sub>	700	0.019	[129]

**Figure 8.** Different types of SOECs. Reproduced with permission from Ref. <sup>[130]</sup>. Copyright 2022, Elsevier.

channels serves to inhibit anode sintering and facilitate the formation of a robust interfacial adhesion, thereby preventing the delamination of anode material during electrolysis<sup>[133]</sup>. In conclusion, FESCs exhibit high electrochemical performance and adaptability to low-temperature operation. The oxygen electrode-supported structure provides an effective approach to preparing SOECs.

### Electrolyte-supported cells

The electrolyte is characterized by robust mechanical properties, facile sintering, and a thickness range of 15–80 μm. The electrolyte, following high-temperature firing, exhibits a denser structure<sup>[134]</sup>. However, an increase in the thickness of the electrolyte layer results in an elevated ohmic resistance of the SOECs, which in turn leads to a decline in the performance of the SOECs. The ionic conductivity of the electrolyte is predominantly temperature-dependent. Higher performance can be achieved at operating temperatures above 800 °C, which constrains the operational range of the electrolytic cell. The current research on ESCs is focused on enhancing ion mobility and reducing electrolyte thickness. Enhancing ion mobility can be achieved by the development of new electrolyte materials, while reducing electrolyte thickness can be accomplished by improvements in the SOEC assembly process.

### DEGRADATION

SOECs exhibit a significant decay in performance over extended periods of operation. The most stable SOEC system exhibits a degradation rate of approximately 3%·(khr)<sup>-1</sup>, which is below the commercial

standard of  $1\% \cdot (\text{hr})^{-1}$ . In order to enhance the stability of the electrolytic cell, it is imperative to gain a comprehensive understanding of the degradation mechanism of the SOEC system<sup>[23]</sup>. It is currently thought that the degradation of the SOEC is mainly associated with the cathode, anode, and electrolyte.

### Cathode degradation

Ni-YSZ exhibits favorable performance in a majority of scenarios. During electrolysis, the primary forms of degradation observed in Ni-YSZ are oxidation, migration, agglomeration, depletion, carbon deposition and poisoning.

The high concentration of steam during the electrolysis process results in the oxidation of Ni particles into gaseous  $\text{Ni}(\text{OH})_x$ , which is subsequently transferred to the surface of the electrolyte. This result increases the ohmic resistance of the electrolytic cell and reduces the TPBs, thereby decreasing the catalytic performance of the electrode materials<sup>[135]</sup>. Furthermore, the formation of NiO results in a reduction in the surface activity and electronic conductivity of the catalyst. Additionally, the formation of NiO dendrites following multiple redox reactions also causes damage to the microstructure of the electrode<sup>[136]</sup>. In order to avoid the oxidation of Ni and enhance the electrochemical performance of the electrodes, the incorporation of partially reducing gases or the doping of metals is typically employed. Chen *et al.* found that Ce could inhibit the oxidation of Ni in  $\text{CO}_2$  [Figure 9A]<sup>[137]</sup>. Accordingly, they prepared a Ce-Ni-YSZ cathode by loading  $\text{Ni}_{0.1}\text{Ce}_{0.9}\text{O}_{2-x}$  nanoparticles on the surface of Ni-YSZ, and observed that its anti- $\text{CO}_2$  oxidation performance was markedly superior to that of Ni-YSZ. This material is a promising cathode for  $\text{CO}_2$  electrolysis.

In addition, Ni-based materials are prone to oxidation during the electrolysis of  $\text{CO}_2$ , resulting in the formation of diverse carbon depositions, including carbon nanotubes, carbon fibers, and amorphous forms. These deposits diminish the area of the TPBs, obstruct the gas transport channels, and compromise the stability of the electrode materials. The doping of Cu can increase the concentration of oxygen vacancies, enhance the conductivity of the material, and accelerate the adsorption and diffusion of  $\text{CO}_2$ <sup>[13]</sup>.

### Anode degradation

SOECs typically require high current densities for optimal performance. At higher current densities ( $> 0.5 \text{ A} \cdot \text{cm}^{-2}$ ), the anode exhibits a more pronounced degradation than the cathode, suggesting that the degradation of SOECs is mainly related to the anode<sup>[138]</sup>. It is commonly believed that delamination at the anode/electrolyte interface, cation migration, and the generation of deleterious phases represent the primary causes of anode degradation.

For LSM-based anode materials, delamination represents a significant factor contributing to the degradation of SOECs. One view is that  $\text{O}_2$  is continuously accumulated at the electrode/electrolyte interface during electrolysis, resulting in the formation of localized high oxygen partial pressure sites that lead to anode delamination [Figure 9B]. Another view is that the cation migration will result in the formation of a secondary phase, which obstructs the active sites on the TPBs, thereby leading to the deterioration of the electrolytic cell. Furthermore, anode poisoning represents another potential cause of SOEC degradation. The interconnects in the SOEC stack are composed of stainless steel. At elevated temperatures, volatile Cr-based compounds, such as  $\text{CrO}_2(\text{OH})_2$ , decompose into  $\text{Cr}_2\text{O}_3$  and other substances that are deposited on the surface of the electrodes and electrolyte<sup>[139]</sup>. This deposition increases the polarization resistance of the electrodes, leading to SOEC degradation<sup>[140]</sup>. In order to mitigate the effects of Cr poisoning, it is common practice to coat conductive materials (e.g., perovskites) on the surface of the interconnects. Sealants and reaction gases typically comprise volatile elements, such as B<sup>[141]</sup> [Figure 9C] and S<sup>[142]</sup>, which can be deposited at the electrode/electrolyte interface. This can block the reaction sites and also damage the pore structure of the electrodes, resulting in a reduction in the catalytic activity and stability of the electrodes.

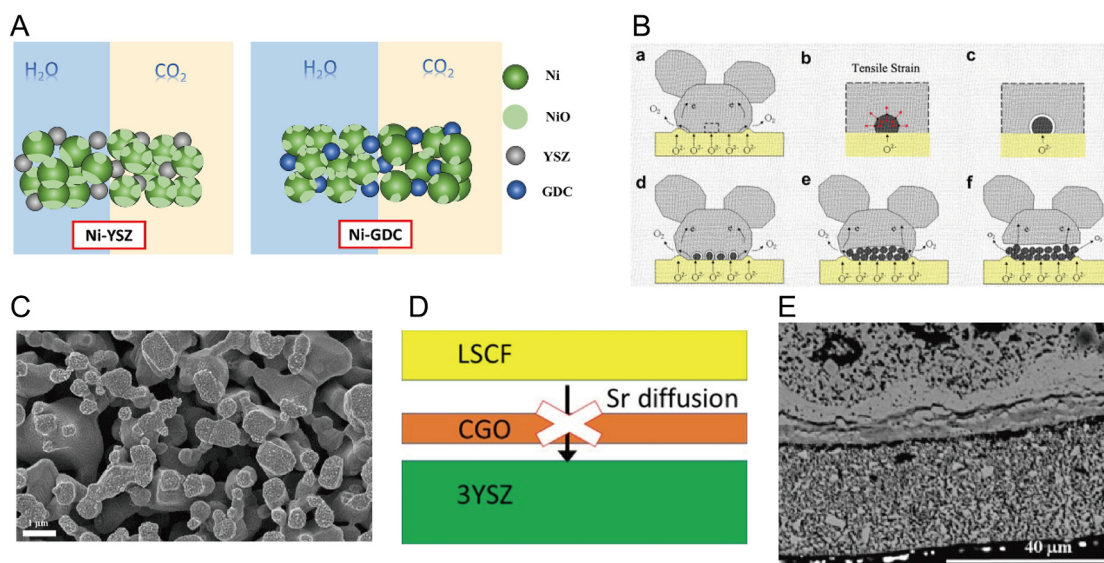


**Figure 9.** (A) Oxidation processes of Ni-YSZ and Ni-GDC in H<sub>2</sub>O and CO<sub>2</sub>. Reproduced with permission from Ref.<sup>[137]</sup>. Copyright 2022, Elsevier. (B) Microstructural changes at the LSM/YSZ interface in SOEC mode. Reproduced with permission from Ref.<sup>[6]</sup>. Copyright 2023, Elsevier. (C) SEM image of the electrode/electrolyte interface after anodic polarization of the LSM for 20 h in the presence of borosilicate glass. Reproduced with permission from Ref.<sup>[141]</sup>. Copyright 2016, Elsevier. (D) Schematic of inhibiting Sr diffusion after adding GDC barrier layer. Reproduced with permission from Ref.<sup>[143]</sup>. Copyright 2021, American Chemical Society. (E) SEM image of YSZ electrolyte rupture. Reproduced with permission from Ref.<sup>[147]</sup>. Copyright 2011, Elsevier.

In LSCF-based materials, cation diffusion and segregation of Sr represent the primary causes of degradation. As shown in Figure 9D, the addition of a GDC barrier layer between the Zr-based solid-state electrolyte and the LSCF can prevent the diffusion of Sr and inhibit the formation of deleterious phases, such as SrZrO<sub>3</sub> or La<sub>2</sub>Zr<sub>2</sub>O<sub>7</sub>. However, this approach was unable to inhibit the degradation of the LSCF<sup>[143]</sup>. Laurencin *et al.* concluded that electrolysis results in the depletion of oxygen vacancies in the LSCF, thereby segregation of Sr from the anode and consequently leading to LSCF degradation<sup>[144]</sup>. However, Ai *et al.* concluded that the direct assembly of LSCF on YSZ without a blocking layer also results in the production of high-performance SOEC anodes<sup>[145]</sup>. It was found that anode polarization has the effect of reducing the concentration of oxygen vacancies and inhibiting the segregation of Sr and the generation of SrZrO<sub>3</sub>, thereby enhancing the stability of the anode/electrolyte interface. The development of innovative material systems and a deeper understanding of the degradation process represent promising avenues for enhancing the stability of SOECs.

### Electrolyte degradation

YSZ may exhibit delamination, fracture, and evolution of metallic elements when subjected to prolonged operation in a reducing atmosphere. Moreover, this material requires high temperatures to sustain its high level of activity, which can result in its degradation and the accelerated aging of sealants. The ohmic resistance in SOECs is attributable to the electrolyte. A reduction in temperature results in a decline of oxygen ion conductivity, which in turn elevates the ohmic resistance and gives rise to fractures at the junctions between electrolyte particles<sup>[146]</sup>. In SOEC mode, Tietz *et al.* found that the electrolyte layer exhibited distinct degradation, with voids forming a clear distribution and horizontally aligned pores at the edges of the electrolyte grains<sup>[65]</sup>. The diffusion of the two elements, Y and Zr, and the crystallization on the electrode surface will result in an increase in the overpotential during the reaction. Laguna-Bercero *et al.*

performed a series of stability tests on a microtubular SOEC with YSZ as the electrolyte at a high voltage of 2.8 V<sup>[147]</sup>. The formation of voids at the grain boundaries of the electrolyte interface results in the propagation of cracks within the electrolyte, leading to delamination, which would impair the performance of the electrolytic cell, as shown in [Figure 9E](#).

ScSZ-based electrolytes exhibit high ionic conductivity at low to medium temperatures (< 800 °C), about twice that of YSZ. However, the grains and grain boundaries of ScSZ are subject to damage during the process of reaction, which in turn affects the conductivity and stability of the electrolyte<sup>[148]</sup>. LSGM exhibits a broad operational temperature range and high ion transfer numbers. However, it displays a discrepancy in thermal expansion coefficients with Ni-based cathode materials, as well as the formation of LaNiO<sub>3</sub> particles during electrolysis, which ultimately results in electrolyte rupture<sup>[149]</sup>. The development of electrolyte materials suitable for low and medium temperatures will be a key area of focus for research.

## STACK AND ECONOMIC BENEFITS

### Structure of stacks

The stacking technology of SOEC is similar to that of SOFC, which is mainly classified into planar<sup>[150]</sup> and tubular<sup>[150]</sup> types [[Figure 10A](#) and [B](#)]. Planar cells are more prevalent in practical applications due to their simple structure, high power density, low internal resistance, and low manufacturing cost<sup>[130]</sup>. However, the fabrication of stacks demands advanced sealing technology and has the risk of gas leakage. The improvement of planar cells is the development of low-cost sealants. Tubular cells exhibit better thermal cycling performance, enhanced structural strength and rapid start/stop capabilities. However, the current trajectory is lengthy, which has resulted in elevated resistance and diminished power density<sup>[94]</sup>. Reducing the inner diameter and preparing microtubular SOECs represents an effective method for enhancing the performance of tubular cells. Yao *et al.* prepared a microtubular SOEC with the structure Ni-YSZ/8YSZ/LSCF-GDC by introducing an insulating ceramic connecting device and employing silver paste as a collector at the cathode [[Figure 10C](#)], which represents a significant improvement compared to that of conventional tubular SOECs<sup>[151]</sup>. The flat-tubular configuration represents a distinctive category of SOEC stacks, which combines the advantages of both planar and tubular SOECs. This configuration offers high power density, robust thermal cycling performance, and ease of sealing, rendering it suitable for industrial applications. As illustrated in [Figure 10D](#), the flat-tubular anode-supported cell without a metal connecting plate can not only avoid Cr poisoning in the reaction process, but also reduce the manufacturing cost, making it a promising candidate for a next-generation SOEC structure<sup>[152]</sup>.

### Economic benefits

Both CO and H<sub>2</sub> are crucial chemical intermediates utilized in the synthesis of a multitude of high-value chemicals, such as ammonia and olefins. At present, the predominant methods of industrial preparation mainly adopt steam methane reforming and coal gasification. The process will result in the generation of a considerable quantity of CO<sub>2</sub> and a notable degree of environmental contamination<sup>[153]</sup>. However, the electrolysis of CO<sub>2</sub> by SOEC to produce CO, not only can directly consume CO<sub>2</sub> in industrial production, but also reduce the consumption of fossil fuels and achieve indirect emission reduction of CO<sub>2</sub>. Blast furnace gas (BFG) is a low calorific value fuel that can be used in a clean and efficient way to produce organic chemicals by CO reduction. However, the use of 'green hydrogen' prepared by SOEC to replace CO can not only reduce environmental pollution, but also greatly improve economic benefits. Kong *et al.* developed a process for value-added recycling of BFG based on BFG-SOFC-SOEC-H<sub>2</sub><sup>[154]</sup>. Optimization was conducted by ASPEN Plus software and the results showed that the process was able to achieve a capture rate of 99.92% of carbon oxides and a hydrogen production rate of 0.24 kmol·(kmol·BFG)<sup>-1</sup>.

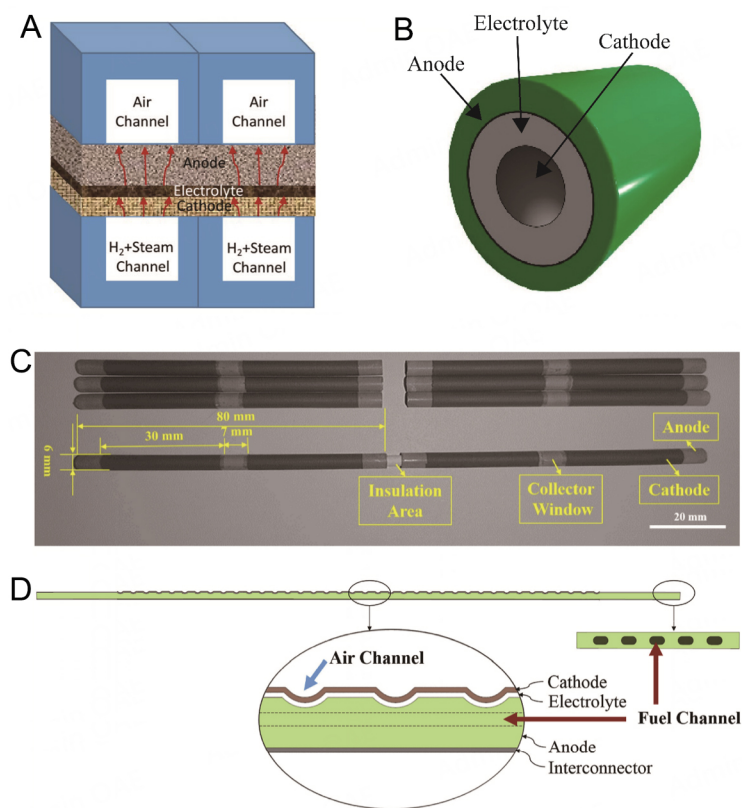


**Figure 10.** (A) A typical planar SOEC stack-unit scheme. Reproduced with permission from Ref.<sup>[150]</sup>. Copyright 2022, MDPI. (B) Schematic of tubular SOEC. Reproduced with permission from Ref.<sup>[130]</sup>. Copyright 2022, Elsevier. (C) Schematic of microtubular SOEC structure. Reproduced with permission from Ref.<sup>[151]</sup>. Copyright 2022, Elsevier. (D) Cross-section of flat-tubular anode-supported cell and channel position. Reproduced with permission from Ref.<sup>[152]</sup>. Copyright 2017, Elsevier.

The economy of SOEC mainly depends on the power consumption in the electrolysis process, and the electrolysis efficiency can be effectively improved by an external heat source. Therefore, fuel-assisted SOEC is proposed to reduce overpotential by adding fuel to the anode, allowing it to react with the generated oxygen. As shown in Figure 11, Xu *et al.* proposed a CH<sub>4</sub>-assisted SOEC co-electrolysis of H<sub>2</sub>O and CO<sub>2</sub> in conjunction with Fischer-Tropsch synthesis for low-carbon feedstock generation<sup>[155]</sup>. It was demonstrated that by modifying the H<sub>2</sub>O/CO<sub>2</sub> ratio at the inlet, it was feasible to regulate the ratio of CO/H<sub>2</sub> in the syngas. This suggests that the SOEC system may offer a significant advantage for hydrocarbon synthesis. Furthermore, the utilization of sine-like flow channels to facilitate the diffusion of reactive gases can serve to enhance the performance and stability of the electrolyzer<sup>[156]</sup>. The combination of this approach with Fischer-Tropsch synthesis represents an additional avenue for the engineering application of SOECs.

## SUMMARY AND OUTLOOK

SOECs, as a high-temperature electrolysis technology, offer a viable approach to energy conversion, storage, and mitigating the greenhouse effect. This paper summarizes the latest research developments in SOECs, emphasizing the materials and degradation mechanisms. Additionally, key challenges that hinder the further advancement of SOECs are also given. We believe that the integration of SOECs with renewable energy sources can facilitate energy storage and ensure a constant output. While significant advancements have been made in the relevant technology, a considerable gap remains between its current state and that of large-scale commercial application. The technical challenges include the degradation of materials due to

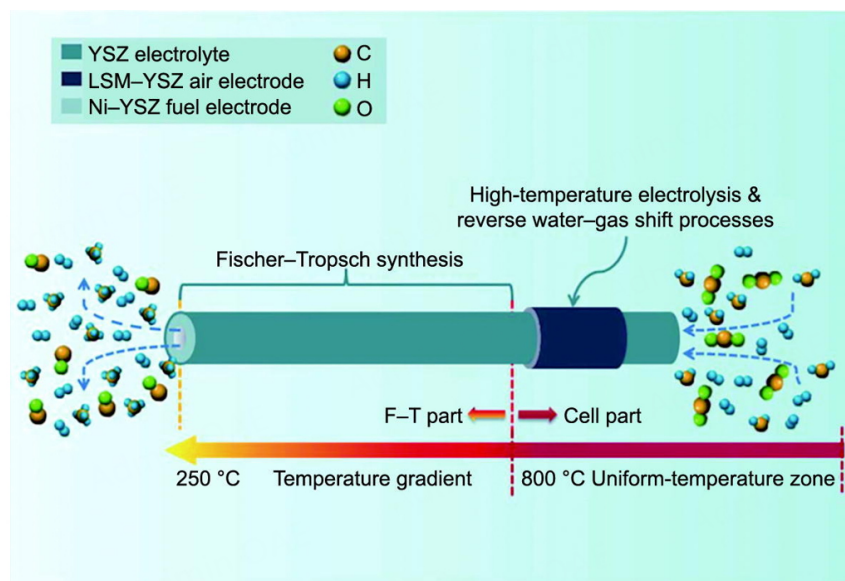


**Figure 11.** Schematic of direct methane synthesis from  $\text{CO}_2\text{-H}_2\text{O}$  co-electrolysis in a tubular unit combining a SOEC and a Fischer-Tropsch reactor. Reproduced with permission from Ref. <sup>[157]</sup>. Copyright 2023, Elsevier.

long-term operation, the development of high-entropy perovskites, the accumulation of harmful substances in interconnect materials, the loss of gas tightness, and the limited scenarios of application. In addition, the economic challenges include higher costs due to reduced durability and increased maintenance costs caused by critical materials such as interconnects and sealants. In summary, to prepare SOECs with good catalytic activity and stability, and promote the industrial application of solid oxide electrolysis technology, future research should focus on the following:

- (1) Developing high-performance electrolyte and electrode materials that are stable at low temperatures while improving the structure of existing materials.
- (2) Enhancing SOEC performance by optimizing the stoichiometric ratio of perovskites and introducing more active sites.
- (3) Advancing H-SOEC technology to enhance its electrocatalytic performance and durability at lower temperatures.
- (4) Exploring new processes to enhance the stack performance, reduce internal resistance, and maintain stable operation under high-temperature conditions.
- (5) Promoting the systematic and large-scale application of SOECs, integrating them with clean energy sources and electric grids.
- (6) Coupling SOECs with other chemical synthesis processes, such as ethylene production from methane or nitrogen monoxide production from nitrogen, to enhance the economic benefits of SOEC technology.
- (7) Conducting in-depth investigations of the mechanisms behind electrolytic reactions and chemical processes at the electrode-electrolyte interface.

(8) Developing an integrated electrolysis and fuel cell system to enhance the flexibility and application scenarios of SOEC technology.

## DECLARATIONS

### Acknowledgments

The authors acknowledge the financial support of the National Key R&D Program of China and the National Natural Science Foundation of China.

### Authors' contributions

Conceived the idea and directed the project: Sun, C.

Wrote the paper: Chen, W.; Sun, C.

### Availability of data and materials

Not applicable.

### Financial support and sponsorship

The financial support of the National Key R&D Program of China (No. 2023YFE0115800) and the National Natural Science Foundation of China (No. 52472271).

### Conflicts of interest

Both authors declared that there are no conflicts of interest.

### Ethical approval and consent to participate

Not applicable.

### Consent for publication

Not applicable.

### Copyright

© The Author(s) 2025.

## REFERENCES

1. Zheng, R.; Liu, Z.; Wang, Y.; Xie, Z.; He, M. The future of green energy and chemicals: rational design of catalysis routes. *Joule* **2022**, *6*, 1148-59. [DOI](#)
2. Wolf, S. E.; Winterhalder, F. E.; Vibhu, V.; et al. Solid oxide electrolysis cells - current material development and industrial application. *J. Mater. Chem. A* **2023**, *11*, 17977-8028. [DOI](#)
3. Hartvigsen, J.; Elangovan, S.; Elwell, J.; Larsen, D. Oxygen production from mars atmosphere carbon dioxide using solid oxide electrolysis. *ECS. Trans.* **2017**, *78*, 2953-63. [DOI](#)
4. Constantin, A. Nuclear hydrogen projects to support clean energy transition: updates on international initiatives and IAEA activities. *Int. J. Hydrogen. Energy* **2024**, *54*, 768-79. [DOI](#)
5. Kumar S, Lim H. An overview of water electrolysis technologies for green hydrogen production. *Energy. Rep.* **2022**, *8*, 13793-813. [DOI](#)
6. Jolaoso, L. A.; Bello, I. T.; Ojelade, O. A.; Yousuf, A.; Duan, C.; Kazempoor, P. Operational and scaling-up barriers of SOEC and mitigation strategies to boost H<sub>2</sub> production- a comprehensive review. *Int. J. Hydrogen. Energy* **2023**, *48*, 33017-41. [DOI](#)
7. Royer, S.; Duprez, D.; Can, F.; et al. Perovskites as substitutes of noble metals for heterogeneous catalysis: dream or reality. *Chem. Rev.* **2014**, *114*, 10292-368. [DOI](#) [PubMed](#)
8. Sun, C.; Alonso, J. A.; Bian, J. Recent advances in perovskite-type oxides for energy conversion and storage applications. *Adv. Energy. Mater.* **2021**, *11*, 2000459. [DOI](#)
9. Lei, L.; Zhang, J.; Yuan, Z.; Liu, J.; Ni, M.; Chen, F. Progress report on proton conducting solid oxide electrolysis cells. *Adv. Funct. Mater.* **2019**, *29*, 1903805. [DOI](#)
10. Guan, S.; Shang, C.; Liu, Z. Resolving the temperature and composition dependence of ion conductivity for yttria-stabilized zirconia from machine learning simulation. *J. Phys. Chem. C* **2020**, *124*, 15085-93. [DOI](#)

11. Liu, Y.; Shao, Z.; Mori, T.; Jiang, S. P. Development of nickel based cermet anode materials in solid oxide fuel cells - now and future. *Mater. Rep. Energy*. **2021**, *1*, 100003. DOI
12. Skafte, T. L.; Guan, Z.; Machala, M. L.; et al. Selective high-temperature CO<sub>2</sub> electrolysis enabled by oxidized carbon intermediates. *Nat. Energy*. **2019**, *4*, 846-55. DOI
13. Opitz, A. K.; Nanning, A.; Rameshan, C.; et al. Surface chemistry of perovskite-type electrodes during high temperature CO<sub>2</sub> electrolysis investigated by operando photoelectron spectroscopy. *ACS. Appl. Mater. Interfaces*. **2017**, *9*, 35847-60. DOI PubMed PMC
14. Tang, Y.; Liu, J. Effect of anode and Boudouard reaction catalysts on the performance of direct carbon solid oxide fuel cells. *Int. J. Hydrogen. Energy*. **2010**, *35*, 11188-93. DOI
15. Yang, Y.; Wang, Y.; Yang, Z.; Chen, Y.; Peng, S. A highly active and durable electrode with in situ exsolved Co nanoparticles for solid oxide electrolysis cells. *J. Power. Sources*. **2020**, *478*, 229082. DOI
16. Wang, S.; Inoishi, A.; Hong, J.; et al. Ni-Fe bimetallic cathodes for intermediate temperature CO<sub>2</sub> electrolyzers using a La<sub>0.9</sub>Sr<sub>0.1</sub>Ga<sub>0.8</sub>Mg<sub>0.2</sub>O<sub>3</sub> electrolyte. *J. Mater. Chem. A*. **2013**, *1*, 12455. DOI
17. Unachukwu, I. D.; Vibhu, V.; Vinke, I. C.; Eichel, R.; de Haart, L. Electrochemical and degradation behaviour of single cells comprising Ni-GDC fuel electrode under high temperature steam- and co-electrolysis conditions. *J. Power. Sources*. **2023**, *556*, 232436. DOI
18. Zheng, M.; Wang, S.; Yang, Y.; Xia, C. Barium carbonate as a synergistic catalyst for the H<sub>2</sub>O/CO<sub>2</sub> reduction reaction at Ni-yttria stabilized zirconia cathodes for solid oxide electrolysis cells. *J. Mater. Chem. A*. **2018**, *6*, 2721-9. DOI
19. Uchida, H.; Nishino, H.; Puengjinda, P.; Kakinuma, K. Remarkably improved durability of Ni-Co dispersed Samaria-doped ceria hydrogen electrodes by reversible cycling operation of solid oxide cells. *J. Electrochem. Soc.* **2020**, *167*, 134516. DOI
20. Puengjinda, P.; Nishino, H.; Kakinuma, K.; Brito, M. E.; Uchida, H. Effect of microstructure on performance of double-layer hydrogen electrodes for reversible SOEC/SOFC. *J. Electrochem. Soc.* **2017**, *164*, F889-94. DOI
21. Zhou, Y.; Wei, F.; Wu, H. Fe-decorated on Sm-doped CeO<sub>2</sub> as cathodes for high-temperature CO<sub>2</sub> electrolysis in solid oxide electrolysis cells. *Electrochim. Acta*. **2022**, *419*, 140434. DOI
22. Kumari, N.; Tiwari, P. K.; Haider, M. A.; Basu, S. Electrochemical performance of infiltrated Cu-GDC and Cu-PDC cathode for CO<sub>2</sub> electrolysis in a solid oxide cell. *ECS. Trans.* **2017**, *78*, 3329-37. DOI
23. Lu, L.; Liu, W.; Wang, J.; et al. Long-term stability of carbon dioxide electrolysis in a large-scale flat-tube solid oxide electrolysis cell based on double-sided air electrodes. *Appl. Energy*. **2020**, *259*, 114130. DOI
24. Ding, S.; Li, M.; Pang, W.; et al. A-site deficient perovskite with nano-socketed Ni-Fe alloy particles as highly active and durable catalyst for high-temperature CO<sub>2</sub> electrolysis. *Electrochim. Acta*. **2020**, *335*, 135683. DOI
25. Deka, D. J.; Kim, J.; Gunduz, S.; Ferree, M.; Co, A. C.; Ozkan, U. S. Temperature-induced changes in the synthesis gas composition in a high-temperature H<sub>2</sub>O and CO<sub>2</sub> co-electrolysis system. *Appl. Catal. A. Gen.* **2020**, *602*, 117697. DOI
26. Jin, C.; Yang, C.; Zhao, F.; Cui, D.; Chen, F. La<sub>0.75</sub>Sr<sub>0.25</sub>Cr<sub>0.5</sub>Mn<sub>0.5</sub>O<sub>3</sub> as hydrogen electrode for solid oxide electrolysis cells. *Int. J. Hydrogen. Energy*. **2011**, *36*, 3340-6. DOI
27. Lay, E.; Gauthier, G.; Dessemond, L. Preliminary studies of the new Ce-doped La/Sr chromo-manganite series as potential SOFC anode or SOEC cathode materials. *Solid. State. Ion.* **2011**, *189*, 91-9. DOI
28. Li, Y.; Gan, Y.; Wang, Y.; Xie, K.; Wu, Y. Composite cathode based on Ni-loaded La<sub>0.75</sub>Sr<sub>0.25</sub>Cr<sub>0.5</sub>Mn<sub>0.5</sub>O<sub>3-δ</sub> for direct steam electrolysis in an oxide-ion-conducting solid oxide electrolyzer. *Int. J. Hydrogen. Energy*. **2013**, *38*, 10196-207. DOI
29. Ruan, C.; Xie, K.; Yang, L.; Ding, B.; Wu, Y. Efficient carbon dioxide electrolysis in a symmetric solid oxide electrolyzer based on nanocatalyst-loaded chromate electrodes. *Int. J. Hydrogen. Energy*. **2014**, *39*, 10338-48. DOI
30. Falcón, H.; Barbero, J. A.; Alonso, J. A.; Martínez-lope, M. J.; Fierro, J. L. G. SrFeO<sub>3-δ</sub> perovskite oxides: chemical features and performance for methane combustion. *Chem. Mater.* **2002**, *14*, 2325-33. DOI
31. Zhu, C.; Hou, S.; Hou, L.; Xie, K. Perovskite SrFeO<sub>3-δ</sub> decorated with Ni nanoparticles for high temperature carbon dioxide electrolysis. *Int. J. Hydrogen. Energy*. **2018**, *43*, 17040-7. DOI
32. Ishihara, T.; Wu, K.; Wang, S. (Invited) High temperature CO<sub>2</sub> electrolysis on La(Sr)Fe(Mn)O<sub>3</sub> oxide cathode by using LaGaO<sub>3</sub> based electrolyte. *ECS. Trans.* **2015**, *66*, 197-205. DOI
33. Zhang, W.; Wei, J.; Yin, F.; Sun, C. Recent advances in carbon-resistant anodes for solid oxide fuel cells. *Mater. Chem. Front.* **2023**, *7*, 1943-91. DOI
34. Li, Y.; Wu, G.; Ruan, C.; et al. Composite cathode based on doped vanadate enhanced with loaded metal nanoparticles for steam electrolysis. *J. Power. Sources*. **2014**, *253*, 349-59. DOI
35. Pudmich, G. Chromite/titanate based perovskites for application as anodes in solid oxide fuel cells. *Solid. State. Ion.* **2000**, *135*, 433-8. DOI
36. Li, Y.; Zhou, J.; Dong, D.; et al. Composite fuel electrode La<sub>0.2</sub>Sr<sub>0.8</sub>TiO<sub>3-δ</sub>-Ce<sub>0.8</sub>Sm<sub>0.2</sub>O<sub>2-δ</sub> for electrolysis of CO<sub>2</sub> in an oxygen-ion conducting solid oxide electrolyser. *Phys. Chem. Chem. Phys.* **2012**, *14*, 15547-53. DOI
37. Yang, L.; Xie, K.; Xu, S.; et al. Redox-reversible niobium-doped strontium titanate decorated with in situ grown nickel nanocatalyst for high-temperature direct steam electrolysis. *Dalton. Trans.* **2014**, *43*, 14147-57. DOI
38. He, B.; Zhao, L.; Song, S.; Liu, T.; Chen, F.; Xia, C. Sr<sub>2</sub>Fe<sub>1.5</sub>Mo<sub>0.5</sub>O<sub>6-δ</sub>-Sm<sub>0.2</sub>Ce<sub>0.8</sub>O<sub>1.9</sub> composite anodes for intermediate-temperature solid oxide fuel cells. *J. Electrochem. Soc.* **2012**, *159*, B619-26. DOI
39. Xi, X.; Liu, J.; Luo, W.; et al. Unraveling the enhanced kinetics of Sr<sub>2</sub>Fe<sub>1+x</sub>Mo<sub>1-x</sub>O<sub>6-δ</sub> electrocatalysts for high-performance solid oxide

- cells. *Adv. Energy Mater.* **2021**, *11*, 2102845. DOI
40. Ge, B.; Ma, J.; Ai, D.; Deng, C.; Lin, X.; Xu, J. Sr<sub>2</sub>FeNbO<sub>6</sub> applied in solid oxide electrolysis cell as the hydrogen electrode: kinetic studies by comparison with Ni-YSZ. *Electrochim. Acta.* **2015**, *151*, 437-46. DOI
41. Zhang, L.; Sun, W.; Xu, C.; et al. Two-fold improvement in chemical adsorption ability to achieve effective carbon dioxide electrolysis. *Appl. Catal. B. Environ.* **2022**, *317*, 121754. DOI
42. Kamlungua, K.; Su, P. Moisture-dependent electrochemical characterization of Ba<sub>0.2</sub>Sr<sub>1.8</sub>Fe<sub>1.5</sub>Mo<sub>0.5</sub>O<sub>6-δ</sub> as the fuel electrode for solid oxide electrolysis cells (SOECs). *Electrochim. Acta.* **2020**, *355*, 136670. DOI
43. Li, Y.; Li, Y.; Wan, Y.; et al. Perovskite oxyfluoride electrode enabling direct electrolyzing carbon dioxide with excellent electrochemical performances. *Adv. Energy Mater.* **2019**, *9*, 1803156. DOI
44. Sengodan, S.; Choi, S.; Jun, A.; et al. Layered oxygen-deficient double perovskite as an efficient and stable anode for direct hydrocarbon solid oxide fuel cells. *Nat. Mater.* **2015**, *14*, 205-9. DOI
45. Lu, C.; Niu, B.; Yi, W.; Ji, Y.; Xu, B. Efficient symmetrical electrodes of PrBaFe<sub>2-x</sub>Co<sub>x</sub>O<sub>5+δ</sub> (x = 0, 0.2, 0.4) for solid oxide fuel cells and solid oxide electrolysis cells. *Electrochim. Acta.* **2020**, *358*, 136916. DOI
46. Qi, W.; Zhang, Y.; Cui, J.; Shu, X.; Wang, Y.; Wu, Y. *In-situ* constructing NiO nanoplatelets network on La<sub>0.75</sub>Sr<sub>0.25</sub>Mn<sub>0.5</sub>Cr<sub>0.5</sub>O<sub>3-δ</sub> electrode with enhanced steam electrolysis. *Int. J. Hydrogen. Energy.* **2017**, *42*, 5657-66. DOI
47. Xu, S.; Chen, S.; Li, M.; Xie, K.; Wang, Y.; Wu, Y. Composite cathode based on Fe-loaded LSCM for steam electrolysis in an oxide-ion-conducting solid oxide electrolyser. *J. Power. Sources.* **2013**, *239*, 332-40. DOI
48. Xu, S.; Dong, D.; Wang, Y.; Doherty, W.; Xie, K.; Wu, Y. Perovskite chromates cathode with resolved and anchored nickel nanoparticles for direct high-temperature steam electrolysis. *J. Power. Sources.* **2014**, *246*, 346-55. DOI
49. Yang, X.; Sun, K.; Ma, M.; et al. Achieving strong chemical adsorption ability for efficient carbon dioxide electrolysis. *Appl. Catal. B. Environ.* **2020**, *272*, 118968. DOI
50. Hosoi, K.; Hagiwara, H.; Ida, S.; Ishihara, T. La<sub>0.8</sub>Sr<sub>0.2</sub>FeO<sub>3-δ</sub> as fuel electrode for solid oxide reversible cells using LaGaO<sub>3</sub>-based oxide electrolyte. *J. Phys. Chem. C.* **2016**, *120*, 16110-7. DOI
51. Tian, Y.; Liu, Y.; Jia, L.; et al. A novel electrode with multifunction and regeneration for highly efficient and stable symmetrical solid oxide cell. *J. Power. Sources.* **2020**, *475*, 228620. DOI
52. Choi, J.; Park, S.; Han, H.; et al. Highly efficient CO<sub>2</sub> electrolysis to CO on Ruddlesden-Popper perovskite oxide with *in situ* exsolved Fe nanoparticles. *J. Mater. Chem. A.* **2021**, *9*, 8740-8. DOI
53. Shin, T. H.; Myung, J. H.; Verbraeken, M.; Kim, G.; Irvine, J. T. Oxygen deficient layered double perovskite as an active cathode for CO<sub>2</sub> electrolysis using a solid oxide conductor. *Faraday. Discuss.* **2015**, *182*, 227-39. DOI
54. Zhang, L.; Zhu, X.; Cao, Z.; et al. Pr and Ti co-doped strontium ferrite as a novel hydrogen electrode for solid oxide electrolysis cell. *Electrochim. Acta.* **2017**, *232*, 542-9. DOI
55. Liu, S.; Liu, Q.; Luo, J. CO<sub>2</sub>-to-CO conversion on layered perovskite with *in situ* exsolved Co-Fe alloy nanoparticles: an active and stable cathode for solid oxide electrolysis cells. *J. Mater. Chem. A.* **2016**, *4*, 17521-8. DOI
56. Tan, T.; Wang, Z.; Qin, M.; et al. *In situ* exsolution of core-shell structured NiFe/FeO<sub>x</sub> nanoparticles on Pr<sub>0.4</sub>Sr<sub>1.6</sub>(NiFe)<sub>1.5</sub>Mo<sub>0.5</sub>O<sub>6-δ</sub> for CO<sub>2</sub> electrolysis. *Adv. Funct. Mater.* **2022**, *32*, 2202878. DOI
57. Wang, S.; Deng, S.; Hao, Z.; Hu, X.; Zheng, Y. Ca/Cu doped SmFeO<sub>3</sub> as a fuel electrode material for direct electrolysis of CO<sub>2</sub> in SOECs. *Fuel. Cells.* **2020**, *20*, 682-9. DOI
58. Zhang, J.; Xie, K.; Wei, H.; et al. *In situ* formation of oxygen vacancy in perovskite Sr<sub>0.95</sub>Ti<sub>0.8</sub>Nb<sub>0.1</sub>M<sub>0.1</sub>O<sub>3</sub> (M = Mn, Cr) toward efficient carbon dioxide electrolysis. *Sci. Rep.* **2014**, *4*, 7082. DOI PubMed PMC
59. Zhang, S.; Wang, H.; Yang, T.; et al. Advanced oxygen-electrode-supported solid oxide electrochemical cells with Sr(Ti, Fe)O<sub>3-δ</sub>-based fuel electrodes for electricity generation and hydrogen production. *J. Mater. Chem. A.* **2020**, *8*, 25867-79. DOI
60. Gao, X.; Ye, L.; Xie, K. Voltage-driven reduction method to optimize *in-situ* exsolution of Fe nanoparticles at Sr<sub>2</sub>Fe<sub>1.5+x</sub>Mo<sub>0.5</sub>O<sub>6-δ</sub> interface. *J. Power. Sources.* **2023**, *561*, 232740. DOI
61. He, F.; Hou, M.; Zhu, F.; et al. Building efficient and durable hetero-interfaces on a perovskite-based electrode for electrochemical CO<sub>2</sub> reduction. *Adv. Energy Mater.* **2022**, *12*, 2202175. DOI
62. Sun, X.; Ye, Y.; Zhou, M.; et al. Layered-perovskite oxides with *in situ* exsolved Co-Fe alloy nanoparticles as highly efficient electrodes for high-temperature carbon dioxide electrolysis. *J. Mater. Chem. A.* **2022**, *10*, 2327-35. DOI
63. Hauch, A.; Kungas, R.; Blennow, P.; et al. Recent advances in solid oxide cell technology for electrolysis. *Science* **2020**, *370*, eaba6118. DOI
64. Jiang, S. P. Development of lanthanum strontium manganite perovskite cathode materials of solid oxide fuel cells: a review. *J. Mater. Sci.* **2008**, *43*, 6799-833. DOI
65. Tietz, F.; Sebold, D.; Brisse, A.; Schefold, J. Degradation phenomena in a solid oxide electrolysis cell after 9000 h of operation. *J. Power. Sources.* **2013**, *223*, 129-35. DOI
66. Su, C.; Lü, Z.; Wang, C.; et al. Effects of a YSZ porous layer between electrolyte and oxygen electrode in solid oxide electrolysis cells on the electrochemical performance and stability. *Int. J. Hydrogen. Energy.* **2019**, *44*, 14493-9. DOI
67. Song, Y.; Zhang, X.; Zhou, Y.; et al. Improving the performance of solid oxide electrolysis cell with gold nanoparticles-modified LSM-YSZ anode. *J. Energy. Chem.* **2019**, *35*, 181-7. DOI
68. Mahata, A.; Datta, P.; Basu, R. N. Synthesis and characterization of Ca doped LaMnO<sub>3</sub> as potential anode material for solid oxide electrolysis cells. *Ceram. Int.* **2017**, *43*, 433-8. DOI

69. Tian, Y.; Li, J.; Liu, Y.; et al. Preparation and properties of  $\text{PrBa}_{0.5}\text{Sr}_{0.5}\text{Co}_{1.5}\text{Fe}_{0.5}\text{O}_{5+\delta}$  as novel oxygen electrode for reversible solid oxide electrochemical cell. *Int. J. Hydrogen. Energy.* **2018**, *43*, 12603-9. DOI
70. Laguna-Bercero, M. A.; Monzón, H.; Larrea, A.; Orera, V. M. Improved stability of reversible solid oxide cells with a nickelate-based oxygen electrode. *J. Mater. Chem. A.* **2016**, *4*, 1446-53. DOI
71. Gu, X.; Nikolla, E. Design of Ruddlesden-popper oxides with optimal surface oxygen exchange properties for oxygen reduction and evolution. *ACS. Catal.* **2017**, *7*, 5912-20. DOI
72. Osinkin, D. A.; Bogdanovich, N. M.; Beresnev, S. M.; Pikalova, E. Y.; Bronin, D. I.; Zaikov, Y. P. Reversible solid oxide fuel cell for power accumulation and generation. *Russ. J. Electrochem.* **2018**, *54*, 644-9. DOI
73. Men, H. J.; Tian, N.; Qu, Y. M.; Wang, M.; Zhao, S.; Yu, J. Improved performance of a lanthanum strontium manganite-based oxygen electrode for an intermediate-temperature solid oxide electrolysis cell realized via ionic conduction enhancement. *Ceram. Int.* **2019**, *45*, 7945-9. DOI
74. Zhang, S.; Wang, H.; Lu, M. Y.; Li, C.; Li, C.; Barnett, S. A. Electrochemical performance and stability of  $\text{SrTi}_{0.3}\text{Fe}_{0.6}\text{Co}_{0.1}\text{O}_{3-\delta}$  infiltrated  $\text{La}_{0.8}\text{Sr}_{0.2}\text{MnO}_3\text{Zr}_{0.92}\text{Y}_{0.16}\text{O}_{2-\delta}$  oxygen electrodes for intermediate-temperature solid oxide electrochemical cells. *J. Power. Sources.* **2019**, *426*, 233-41. DOI
75. Yan, J.; Zhao, Z.; Shang, L.; Ou, D.; Cheng, M. Co-synthesized Y-stabilized  $\text{Bi}_2\text{O}_3$  and Sr-substituted  $\text{LaMnO}_3$  composite anode for high performance solid oxide electrolysis cell. *J. Power. Sources.* **2016**, *319*, 124-30. DOI
76. Peng, X.; Tian, Y.; Liu, Y.; et al. An efficient symmetrical solid oxide electrolysis cell with LSCFM-based electrodes for direct electrolysis of pure  $\text{CO}_2$ . *J. Co2. Util.* **2020**, *36*, 18-24. DOI
77. Fan, H.; Zhang, Y.; Han, M. Infiltration of  $\text{La}_{0.6}\text{Sr}_{0.4}\text{FeO}_{3-\delta}$  nanoparticles into YSZ scaffold for solid oxide fuel cell and solid oxide electrolysis cell. *J. Alloys. Compd.* **2017**, *723*, 620-6. DOI
78. Vibhu, V.; Vinke, I. C.; Zaravelis, F.; et al. Performance and degradation of electrolyte-supported single cell composed of Mo-Au-Ni/GDC fuel electrode and LSCF oxygen electrode during high temperature steam electrolysis. *Energies* **2022**, *15*, 2726. DOI
79. Sar, J.; Schefold, J.; Brisse, A.; Djurado, E. Durability test on coral  $\text{Ce}_{0.9}\text{Gd}_{0.1}\text{O}_{2-\delta}$ - $\text{La}_{0.6}\text{Sr}_{0.4}\text{Co}_{0.2}\text{Fe}_{0.8}\text{O}_{3-\delta}$  with  $\text{La}_{0.6}\text{Sr}_{0.4}\text{Co}_{0.2}\text{Fe}_{0.8}\text{O}_{3-\delta}$  current collector working in SOFC and SOEC modes. *Electrochim. Acta.* **2016**, *201*, 57-69. DOI
80. Yang, Z.; Wang, N.; Ma, C.; et al. Co-electrolysis of  $\text{H}_2\text{O}-\text{CO}_2$  in a solid oxide electrolysis cell with symmetrical  $\text{La}_{0.4}\text{Sr}_{0.6}\text{Co}_{0.2}\text{Fe}_{0.7}\text{Nb}_{0.1}\text{O}_{3-\delta}$  electrode. *J. Electroanal. Chem.* **2019**, *836*, 107-11. DOI
81. Cao, Z.; Wei, B.; Miao, J.; et al. Efficient electrolysis of  $\text{CO}_2$  in symmetrical solid oxide electrolysis cell with highly active  $\text{La}_{0.3}\text{Sr}_{0.7}\text{Fe}_{0.7}\text{Ti}_{0.3}\text{O}_3$  electrode material. *Electrochem. Commun.* **2016**, *69*, 80-3. DOI
82. Dey, S.; Mukhopadhyay, J.; Lenka, R. K.; et al. Synthesis and characterization of Nanocrystalline  $\text{Ba}_{0.6}\text{Sr}_{0.4}\text{Co}_{0.8}\text{Fe}_{0.2}\text{O}_3$  for application as an efficient anode in solid oxide electrolyser cell. *Int. J. Hydrogen. Energy.* **2020**, *45*, 3995-4007. DOI
83. Meng, X.; Shen, Y.; Xie, M.; et al. Novel solid oxide cells with  $\text{SrCo}_{0.8}\text{Fe}_{0.1}\text{Ga}_{0.1}\text{O}_{3-\delta}$  oxygen electrode for flexible power generation and hydrogen production. *J. Power. Sources.* **2016**, *306*, 226-32. DOI
84. Zhao, Z.; Qi, H.; Tang, S.; et al. A highly active and stable hybrid oxygen electrode for reversible solid oxide cells. *Int. J. Hydrogen. Energy.* **2021**, *46*, 36012-22. DOI
85. Ni, C.; Irvine, J. T. Calcium manganite as oxygen electrode materials for reversible solid oxide fuel cell. *Faraday. Discuss.* **2015**, *182*, 289-305. DOI PubMed
86. Li, J.; Zhong, C.; Meng, X.; et al.  $\text{Sr}_2\text{Fe}_{1.5}\text{Mo}_{0.5}\text{O}_{6-\delta}-\text{Zr}_{0.84}\text{Y}_{0.16}\text{O}_{2-\delta}$  materials as oxygen electrodes for solid oxide electrolysis cells. *Fuel. Cells.* **2014**, *14*, 1046-9. DOI
87. Tong, X.; Zhou, F.; Yang, S.; Zhong, S.; Wei, M.; Liu, Y. Performance and stability of Ruddlesden-Popper  $\text{La}_2\text{NiO}_{4+\delta}$  oxygen electrodes under solid oxide electrolysis cell operation conditions. *Ceram. Int.* **2017**, *43*, 10927-33. DOI
88. Ren, C.; Gan, Y.; Yang, C.; Lee, M.; Green, R. D.; Xue, X. Fabrication and characterization of microtubular solid oxide cells for  $\text{CO}_2$ /CO redox operations. *J. Appl. Electrochem.* **2018**, *48*, 959-71. DOI
89. Danilov, N.; Lyagaeva, J.; Vdovin, G.; Pikalova, E.; Medvedev, D. Electricity/hydrogen conversion by the means of a protonic ceramic electrolysis cell with  $\text{Nd}_2\text{NiO}_{4+\delta}$ -based oxygen electrode. *Energy. Convers. Manag.* **2018**, *172*, 129-37. DOI
90. Morales-Zapata, M.; Larrea, A.; Laguna-Bercero, M. Reversible operation performance of microtubular solid oxide cells with a nickelate-based oxygen electrode. *Int. J. Hydrogen. Energy.* **2020**, *45*, 5535-42. DOI
91. Zhang, M.; Wang, E.; Mao, J.; Wang, H.; Ouyang, M.; Hu, H. Performance analysis of a metal-supported intermediate-temperature solid oxide electrolysis cell. *Front. Energy. Res.* **2022**, *10*, 888787. DOI
92. Wu, T.; Zhang, W.; Li, Y.; et al. Micro-/nanohoneycomb solid oxide electrolysis cell anodes with ultralarge current tolerance. *Adv. Energy. Mater.* **2018**, *8*, 1802203. DOI
93. Cao, J.; Li, Y.; Zheng, Y.; et al. A novel solid oxide electrolysis cell with micro-/nano channel anode for electrolysis at ultra-high current density over  $5 \text{ A cm}^{-2}$ . *Adv. Energy. Mater.* **2022**, *12*, 2200899. DOI
94. Sahu, S. K.; Panthi, D.; Soliman, I.; Feng, H.; Du, Y. Fabrication and performance of micro-tubular solid oxide cells. *Energies* **2022**, *15*, 3536. DOI
95. Gaikwad, P. S.; Mondal, K.; Shin, Y. K.; van, D. A. C. T.; Pawar, G. Enhancing the Faradaic efficiency of solid oxide electrolysis cells: progress and perspective. *NPJ. Comput. Mater.* **2023**, *9*, 1044. DOI
96. Brett, D. J.; Atkinson, A.; Brandon, N. P.; Skinner, S. J. Intermediate temperature solid oxide fuel cells. *Chem. Soc. Rev.* **2008**, *37*, 1568-78. DOI PubMed
97. Kim, C.; Park, K.; Kalaev, D.; Nicollet, C.; Tuller, H. L. Effect of structure on oxygen diffusivity in layered oxides: a combined

- theoretical and experimental study. *J. Mater. Chem. A*. **2022**, *10*, 15402-14. DOI
98. Abdullah, B. J.; Jiang, Q.; Omar, M. S. Effects of size on mass density and its influence on mechanical and thermal properties of ZrO<sub>2</sub> nanoparticles in different structures. *Bull. Mater. Sci.* **2016**, *39*, 1295-302. DOI
99. Shi, H.; Su, C.; Ran, R.; Cao, J.; Shao, Z. Electrolyte materials for intermediate-temperature solid oxide fuel cells. *Prog. Nat. Sci. Mater. Int.* **2020**, *30*, 764-74. DOI
100. Vendrell, X.; Yadav, D.; Raj, R.; West, A. R. Influence of flash sintering on the ionic conductivity of 8 mol% yttria stabilized zirconia. *J. Eur. Ceram. Soc.* **2019**, *39*, 1352-8. DOI
101. Mineshige, A. Preparation of dense electrolyte layer using dissociated oxygen electrochemical vapor deposition technique. *Solid. State. Ion.* **2004**, *175*, 483-5. DOI
102. Zhang, Y.; Huang, X.; Lu, Z.; et al. Effect of starting powder on screen-printed YSZ films used as electrolyte in SOFCs. *Solid. State. Ion.* **2006**, *177*, 281-7. DOI
103. Yu, B.; Zhang, W.; Xu, J.; Chen, J.; Luo, X.; Stephan, K. Preparation and electrochemical behavior of dense YSZ film for SOEC. *Int. J. Hydrogen. Energy.* **2012**, *37*, 12074-80. DOI
104. Ye, L.; Xie, K. High-temperature electrocatalysis and key materials in solid oxide electrolysis cells. *J. Energy. Chem.* **2021**, *54*, 736-45. DOI
105. Kumar C, Bauri R. Enhancing the phase stability and ionic conductivity of scandia stabilized zirconia by rare earth co-doping. *J. Phys. Chem. Solids.* **2014**, *75*, 642-50. DOI
106. Bernadet, L.; Moncasi, C.; Torrell, M.; Tarancón, A. High-performing electrolyte-supported symmetrical solid oxide electrolysis cells operating under steam electrolysis and co-electrolysis modes. *Int. J. Hydrogen. Energy.* **2020**, *45*, 14208-17. DOI
107. Puente-Martínez, D.; Díaz-Guillén, J.; Montemayor, S.; et al. High ionic conductivity in CeO<sub>2</sub> SOFC solid electrolytes; effect of Dy doping on their electrical properties. *Int. J. Hydrogen. Energy.* **2020**, *45*, 14062-70. DOI
108. Molenda, J.; Świerczek, K.; Zając, W. Functional materials for the IT-SOFC. *J. Power. Sources.* **2007**, *173*, 657-70. DOI
109. Wang, J.; Xiao, X.; Liu, Y.; Pan, K.; Pang, H.; Wei, S. The application of CeO<sub>2</sub>-based materials in electrocatalysis. *J. Mater. Chem. A.* **2019**, *7*, 17675-702. DOI
110. Zhang, Y.; Zhao, S.; Feng, J.; et al. Unraveling the physical chemistry and materials science of CeO<sub>2</sub>-based nanostructures. *Chem* **2021**, *7*, 2022-59. DOI
111. Qian, J.; Gong, Z.; Wang, M.; et al. Generating an electron-blocking layer with BaMn<sub>1-x</sub>Ni<sub>x</sub>O<sub>3</sub> mixed-oxide for Ce<sub>0.8</sub>Sm<sub>0.2</sub>O<sub>2-δ</sub>-based solid oxide fuel cells. *Ceram. Int.* **2018**, *44*, 12739-44. DOI
112. Ishihara, T.; Matsuda, H.; Takita, Y. Doped LaGaO<sub>3</sub> perovskite type oxide as a new oxide ionic conductor. *J. Am. Chem. Soc.* **1994**, *116*, 3801-3. DOI
113. Yi, J. Y.; Choi, G. M. The effect of reduction atmosphere on the LaGaO<sub>3</sub>-based solid oxide fuel cell. *J. Eur. Ceram. Soc.* **2005**, *25*, 2655-9. DOI
114. Tan, Z.; Ishihara, T. Effect of Ni-based cathodic layer on intermediate temperature tubular electrolysis cell using LaGaO<sub>3</sub>-based electrolyte thin film. *J. Phys. Energy.* **2020**, *2*, 024004. DOI
115. Dudek, M.; Lis, B.; Rapacz-Kmita, A.; Gajek, M.; Raźniak, A.; Drożdż, E. Some observations on the synthesis and electrolytic properties of (Ba<sub>1-x</sub>Ca<sub>x</sub>)(M<sub>0.9</sub>Y<sub>0.1</sub>)O<sub>3</sub>, M=Ce, Zr-based samples modified with calcium. *Mater. Sci. Poland.* **2016**, *34*, 101-14. DOI
116. Katahira, K.; Kohchi, Y.; Shimura, T.; Iwahara, H. Protonic conduction in Zr-substituted BaCeO<sub>3</sub>. *Solid. State. Ion.* **2000**, *138*, 91-8. DOI
117. Yang, L.; Wang, S.; Blinn, K.; et al. Enhanced sulfur and coking tolerance of a mixed ion conductor for SOFCs: BaZr<sub>0.1</sub>Ce<sub>0.7</sub>Y<sub>0.2-x</sub>Yb<sub>x</sub>O<sub>3-δ</sub>. *Science* **2009**, *326*, 126-9. DOI
118. Rajendran, S.; Thangavel, N. K.; Ding, H.; Ding, Y.; Ding, D.; Reddy, A. L. M. Tri-doped BaCeO<sub>3</sub>-BaZrO<sub>3</sub> as a chemically stable electrolyte with high proton-conductivity for intermediate temperature solid oxide electrolysis cells (SOECs). *ACS. Appl. Mater. Interfaces.* **2020**, *12*, 38275-84. DOI
119. Li, W.; Guan, B.; Ma, L.; Tian, H.; Liu, X. Synergistic coupling of proton conductors BaZr<sub>0.1</sub>Ce<sub>0.7</sub>Y<sub>0.1</sub>Yb<sub>0.1</sub>O<sub>3-δ</sub> and La<sub>2</sub>Ce<sub>2</sub>O<sub>7</sub> to create chemical stable, interface active electrolyte for steam electrolysis cells. *ACS. Appl. Mater. Interfaces.* **2019**, *11*, 18323-30. DOI
120. Kim, J.; Jun, A.; Gwon, O.; et al. Hybrid-solid oxide electrolysis cell: a new strategy for efficient hydrogen production. *Nano. Energy.* **2018**, *44*, 121-6. DOI
121. Xue, Q.; Huang, X.; Zhang, H.; Xu, H.; Zhang, J.; Wang, L. Synthesis and characterization of high ionic conductivity ScSZ core/shell nanocomposites. *J. Rare. Earths.* **2017**, *35*, 567-73. DOI
122. Matsui, T.; Inaba, M.; Mineshige, A.; Ogumi, Z. Electrochemical properties of ceria-based oxides for use in intermediate-temperature SOFCs. *Solid. State. Ion.* **2005**, *176*, 647-54. DOI
123. Hirano, M. Effect of Bi<sub>2</sub>O<sub>3</sub> additives in Sc stabilized zirconia electrolyte on a stability of crystal phase and electrolyte properties. *Solid. State. Ion.* **2003**, *158*, 215-23. DOI
124. Traina, K.; Henrist, C.; Vertruyen, B.; Cloots, R. Dense La<sub>0.9</sub>Sr<sub>0.1</sub>Ga<sub>0.8</sub>Mg<sub>0.2</sub>O<sub>2.85</sub> electrolyte for IT-SOFC's: sintering study and electrochemical characterization. *J. Alloys. Compd.* **2011**, *509*, 1493-500. DOI
125. Biswal, R. C.; Biswas, K. Novel way of phase stability of LSGM and its conductivity enhancement. *Int. J. Hydrogen. Energy.* **2015**, *40*, 509-18. DOI
126. Rao, Y.; Zhong, S.; He, F.; Wang, Z.; Peng, R.; Lu, Y. Cobalt-doped BaZrO<sub>3</sub>: a single phase air electrode material for reversible solid oxide cells. *Int. J. Hydrogen. Energy.* **2012**, *37*, 12522-7. DOI

127. Lyagaeva, J.; Danilov, N.; Vdovin, G.; et al. A new Dy-doped BaCeO<sub>3</sub>-BaZrO<sub>3</sub> proton-conducting material as a promising electrolyte for reversible solid oxide fuel cells. *J. Mater. Chem. A*. **2016**, *4*, 15390-9. DOI
128. Yang, S.; Wen, Y.; Zhang, S.; Gu, S.; Wen, Z.; Ye, X. Performance and stability of BaCe<sub>0.8-x</sub>Zr<sub>0.2</sub>In<sub>x</sub>O<sub>3-δ</sub>-based materials and reversible solid oxide cells working at intermediate temperature. *Int. J. Hydrogen. Energy*. **2017**, *42*, 28549-58. DOI
129. Yang, S.; Zhang, S.; Sun, C.; Ye, X.; Wen, Z. Lattice incorporation of Cu<sup>2+</sup> into the BaCe<sub>0.7</sub>Zr<sub>0.1</sub>Y<sub>0.1</sub>Yb<sub>0.1</sub>O<sub>3-δ</sub> electrolyte on boosting its sintering and proton-conducting abilities for reversible solid oxide cells. *ACS. Appl. Mater. Interfaces*. **2018**, *10*, 42387-96. DOI
130. Golkhatmi S, Asghar MI, Lund PD. A review on solid oxide fuel cell durability: latest progress, mechanisms, and study tools. *Renew. Sustain. Energy. Rev.* **2022**, *161*, 112339. DOI
131. Park, S.; Craciun, R.; Vohs, J. M.; Gorte, R. J. Direct oxidation of hydrocarbons in a solid oxide fuel cell: I. methane oxidation. *J. Electrochem. Soc.* **1999**, *146*, 3603-5. DOI
132. Wehrle, L.; Schmider, D.; Dailly, J.; Banerjee, A.; Deutschmann, O. Benchmarking solid oxide electrolysis cell-stacks for industrial Power-to-Methane systems via hierarchical multi-scale modelling. *Appl. Energy*. **2022**, *317*, 119143. DOI
133. Li, T.; Wang, T.; Wei, T.; et al. Robust anode-supported cells with fast oxygen release channels for efficient and stable CO<sub>2</sub> electrolysis at ultrahigh current densities. *Small* **2021**, *17*, e2007211. DOI
134. Zhou, J.; Ma, Z.; Zhang, L.; et al. Study of CO<sub>2</sub> and H<sub>2</sub>O direct co-electrolysis in an electrolyte-supported solid oxide electrolysis cell by aqueous tape casting technique. *Int. J. Hydrogen. Energy*. **2019**, *44*, 28939-46. DOI
135. Rorato, L.; Shang, Y.; Yang, S.; et al. Understanding the Ni migration in solid oxide cell: a coupled experimental and modeling approach. *J. Electrochem. Soc.* **2023**, *170*, 034504. DOI
136. Dasari, H. P.; Park, S.; Kim, J.; et al. Electrochemical characterization of Ni-yttria stabilized zirconia electrode for hydrogen production in solid oxide electrolysis cells. *J. Power. Sources*. **2013**, *240*, 721-8. DOI
137. Chen, D.; Barreau, M.; Dintzer, T.; et al. Surface oxidation of Ni-cermet electrodes by CO<sub>2</sub> and H<sub>2</sub>O and how to moderate it. *J. Energy. Chem.* **2022**, *67*, 300-8. DOI
138. Graves, C.; Ebbesen, S. D.; Mogensen, M. Co-electrolysis of CO<sub>2</sub> and H<sub>2</sub>O in solid oxide cells: performance and durability. *Solid. State. Ion.* **2011**, *192*, 398-403. DOI
139. Min, K.; Sun, C. W.; Qu, W.; et al. Electrochemical properties of low-temperature solid oxide fuel cells under chromium poisoning conditions. *Int. J. Green. Energy*. **2009**, *6*, 627-37. DOI
140. Bi, J.; Yang, S.; Zhong, S.; et al. An insight into the effects of B-site transition metals on the activity, activation effect and stability of perovskite oxygen electrodes for solid oxide electrolysis cells. *J. Power. Sources*. **2017**, *363*, 470-9. DOI
141. Chen, K.; Hyodo, J.; Ai, N.; Ishihara, T.; Jiang, S. P. Boron deposition and poisoning of La<sub>0.8</sub>Sr<sub>0.2</sub>MnO<sub>3</sub> oxygen electrodes of solid oxide electrolysis cells under accelerated operation conditions. *Int. J. Hydrogen. Energy*. **2016**, *41*, 1419-31. DOI
142. Wang, C. C.; Chen, K.; Jiang, T.; et al. Sulphur poisoning of solid oxide electrolysis cell anodes. *Electrochim. Acta*. **2018**, *269*, 188-95. DOI
143. Riegraf, M.; Han, F.; Sata, N.; Costa, R. Intercalation of thin-film Gd-doped ceria barrier layers in electrolyte-supported solid oxide cells: physicochemical aspects. *ACS. Appl. Mater. Interfaces*. **2021**, *13*, 37239-51. DOI PubMed
144. Laurencin, J.; Hubert, M.; Sanchez, D. F.; et al. Degradation mechanism of La<sub>0.6</sub>Sr<sub>0.4</sub>Co<sub>0.2</sub>Fe<sub>0.8</sub>O<sub>3-δ</sub>/Gd<sub>0.1</sub>Ce<sub>0.9</sub>O<sub>2-δ</sub> composite electrode operated under solid oxide electrolysis and fuel cell conditions. *Electrochim. Acta*. **2017**, *241*, 459-76. DOI
145. Ai, N.; He, S.; Li, N.; et al. Suppressed Sr segregation and performance of directly assembled La<sub>0.6</sub>Sr<sub>0.4</sub>Co<sub>0.2</sub>Fe<sub>0.8</sub>O<sub>3-δ</sub> oxygen electrode on Y<sub>2</sub>O<sub>3</sub>-ZrO<sub>2</sub> electrolyte of solid oxide electrolysis cells. *J. Power. Sources*. **2018**, *384*, 125-35. DOI
146. Kim, J.; Ji, H.; Dasari, H. P.; et al. Degradation mechanism of electrolyte and air electrode in solid oxide electrolysis cells operating at high polarization. *Int. J. Hydrogen. Energy*. **2013**, *38*, 1225-35. DOI
147. Laguna-Bercero, M.; Campana, R.; Larrea, A.; Kilner, J.; Orera, V. Electrolyte degradation in anode supported microtubular yttria stabilized zirconia-based solid oxide steam electrolysis cells at high voltages of operation. *J. Power. Sources*. **2011**, *196*, 8942-7. DOI
148. Zakaria, Z.; Kamarudin, S. K. Advanced modification of scandia-stabilized zirconia electrolytes for solid oxide fuel cells application-A review. *Int. J. Energy. Res.* **2021**, *45*, 4871-87. DOI
149. Laguna-bercero, M. Recent advances in high temperature electrolysis using solid oxide fuel cells: a review. *J. Power. Sources*. **2012**, *203*, 4-16. DOI
150. Zhang, Z.; Guan, C.; Xie, L.; Wang, J. Design and analysis of a novel opposite trapezoidal flow channel for solid oxide electrolysis cell stack. *Energies* **2023**, *16*, 159. DOI
151. Yao, Y.; Ma, Y.; Wang, C.; et al. A cofuel channel microtubular solid oxide fuel/electrolysis cell. *Appl. Energy*. **2022**, *327*, 120010. DOI
152. Park, S.; Sammes, N. M.; Song, K.; Kim, T.; Chung, J. Monolithic flat tubular types of solid oxide fuel cells with integrated electrode and gas channels. *Int. J. Hydrogen. Energy*. **2017**, *42*, 1154-60. DOI
153. Houaijia, A.; Breuer, S.; Thomey, D.; et al. Solar hydrogen by high-temperature electrolysis: flowsheeting and experimental analysis of a tube-type receiver concept for superheated steam production. *Energy. Procedia*. **2014**, *49*, 1960-9. DOI
154. Kong, R.; Zhang, R.; Li, H.; Wu, Y.; Sun, Z.; Sun, Z. A new pathway to produce hydrogen with CO capture from blast furnace gas via SOFC-SOEC integration. *Energy. Convers. Manag.* **2022**, *271*, 116278. DOI
155. Xu, H.; Maroto-Valer, M. M.; Ni, M.; Cao, J.; Xuan, J. Low carbon fuel production from combined solid oxide CO<sub>2</sub> co-electrolysis and Fischer-Tropsch synthesis system: a modelling study. *Appl. Energy*. **2019**, *242*, 911-8. DOI

156. Xu, Y.; Cai, S.; Chi, B.; Tu, Z. Numerical study on improved mass and heat transfer performance in a solid oxide electrolysis cell with sine wave flow field. *Int. J. Hydrogen. Energy.* **2024**. DOI
157. Li, Y.; Zhang, L.; Yu, B.; Zhu, J.; Wu, C. CO<sub>2</sub> high-temperature electrolysis technology toward carbon neutralization in the chemical industry. *Engineering* **2023**, *21*, 101-14. DOI